General Disclaimer

One or more of the Following Statements may affect this Document

- This document has been reproduced from the best copy furnished by the organizational source. It is being released in the interest of making available as much information as possible.

- This document may contain data, which exceeds the sheet parameters. It was furnished in this condition by the organizational source and is the best copy available.

- This document may contain tone-on-tone or color graphs, charts and/or pictures, which have been reproduced in black and white.

- This document is paginated as submitted by the original source.

- Portions of this document are not fully legible due to the historical nature of some of the material. However, it is the best reproduction available from the original submission.

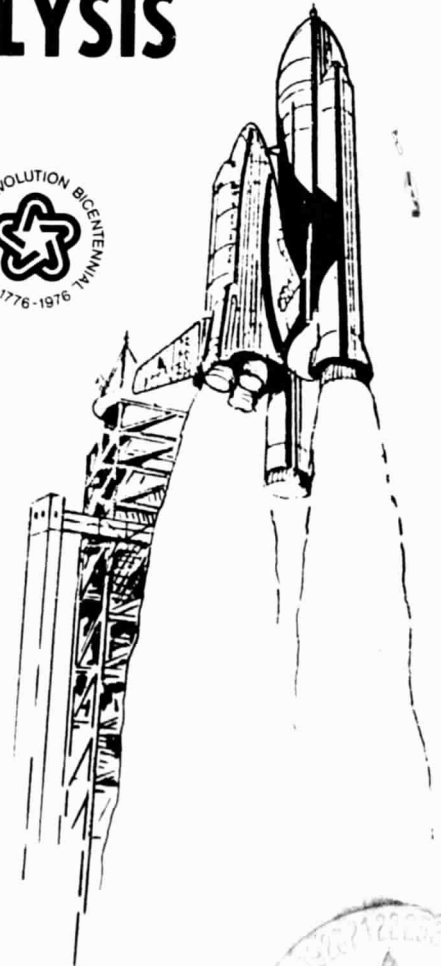Produced by the NASA Center for Aerospace Information (CASI)

LMSC-HREC TM D496636

LOCKHEED

147528

SPACE SHUTTLE SRM PLUME EXPANSION SENSITIVITY ANALYSIS

November 1975

Contract NAS9-14517

AMERICAN REVOLUTION BICENTENNIAL
1776-1976

Prepared for

National Aeronautics and Space Administration
Aerodynamic Systems Analysis Section
Johnson Space Center, Houston, TX 77058

by

Sheldon D. Smith
James A. Tevepaugh
Morris M. Penny

Lockheed Missiles & Space Company, Inc.
Huntsville Research & Engineering Center
4800 Bradford Drive, Huntsville, AL 35807

APR 1976
RECEIVED
NASA STI FACILITY
INPUT BRANCH

FOREWORD

This document presents the results of an analysis performed by personnel of the Lockheed-Huntsville Research & Engineering Center for the Aerodynamic Systems Analysis Section of the Johnson Space Center, Houston, Texas, under Contract NAS9-14517. The work was performed in support of an analysis of the Space Shuttle solid rocket motor exhaust plumes.

SUMMARY

A parametric analysis was conducted to assess the sensitivity of the initial plume expansion angle of analytical solid rocket motor flow fields to various analytical input parameters and operating conditions. The results of the analysis are presented and conclusions reached regarding the sensitivity of the initial plume expansion angle to each parameter investigated. Operating conditions parametrically varied were chamber pressure, nozzle inlet angle, nozzle throat radius of curvature ratio and propellant particle loading. Empirical particle parameters investigated were mean size, local drag coefficient and local heat transfer coefficient. Sensitivity of the initial plume expansion angle to gas thermochemistry model and local drag coefficient model assumptions were determined. Initial plume expansion angle was most sensitive to gas thermochemistry model, propellant particle loading, and mean particle size assumption. Initial plume expansion angle was minimally sensitive to chamber pressure, nozzle throat radius of curvature ratio, nozzle inlet angle, local drag coefficient and local heat transfer coefficient. The local drag coefficient model assumption had no effect on the initial plume expansion angle.

CONTENTS

TABLE

LIST OF FIGURES

v

LIST OF FIGURES (Continued)

LIST OF FIGURES (Concluded)

NOMENCLATURE

Symbol	Description
A/A^*	nozzle area ratio
C_D	particle drag coefficient
C_{P_L}	particle specific heat at constant pressure for liquid phase at melting temperature
C_{P_S}	particle specific heat at constant pressure for solid phase at melting temperature
H_{P_L}	particle enthalpy for liquid phase at melting temperature
H_{P_S}	particle enthalpy for solid phase at melting temperature
M	Mach number
M_W	molecular weight
Q	particle heat transfer coefficient
P	pressure
r_{mp}	particle radius
R_c/R_t	ratio of throat radius of curvature to nozzle throat radius
T	gas static temperature
$\dot{\omega}_p/\dot{\omega}_g$	ratio of particle mass flow rate to gas mass flow rate

Greek

γ	ratio of specific heats
δ_j	initial plume expansion angle
θ_{lip}	nozzle lip angle
θ_I	nozzle inlet angle

Subscripts

c	chamber condition
e	exit plane condition
∞	ambient freestream

viii

Section 1
INTRODUCTION

The exhaust plumes of the Space Shuttle solid rocket motors (SRMs) can have a significant effect (Ref. 1) on the base pressure and base drag of the Shuttle vehicle. Previous studies (Ref. 2) have shown that base pressure can be correlated to the initial plume expansion angle, δ_j. These same studies indicate that small changes in δ_j can have a significant effect on the vehicle base pressure. Therefore, it is necessary to predict the value of δ_j as accurately as possible before a realistic assessment of the exhaust plume effect on the vehicle base pressure can be ascertained.

Prediction of δ_j requires that the nozzle exit conditions be known. This requires a definition of the nozzle flow field which is a function of the nozzle geometry, chamber operating conditions and particulate behavior. Nozzle geometry is described by analytic functions. The chamber operating conditions are obtained from analytical combustion models which utilize the propellant formulation and combustion pressure. However; the particle data (size, drag, heat transfer) are described empirically. Since the plume initial expansion angle has been shown to be an important correlation parameter for vehicle base drag, relevant questions are how does the empiricism affect the flow field and how sensivitive is δ_j to the input data? These questions were the subject of an investigation which parametrically examined the sensitivity of δ_j to the various input data. Input parameters examined included:

1. Chamber Pressure
2. Flowfield Chemistry Assumption
3. Particle Loading
4. Particle Size
5. Particle Drag Coefficient

6. Particle Heat Transfer Coefficient, and

7. Nozzle Geometric Modifications.

The discussion is begun with a description of the nominal set of input and operating parameters for the nozzle solution.

This report describes the results of this investigation.

Section 2
DISCUSSION

2.1 NOZZLE FLOWFIELD ANALYSIS

The Space Shuttle SRM utilizes a solid propellant which contains 16% by weight of aluminum. The presence of the aluminum results in the formation of aluminum oxide (Al_2O_3) particulates in the exhaust. For the heavily aluminum loaded SRM propellant the two-phase effects on the gaseous expansion process are significant. Therefore, it is important that the analytic solution of the nozzle and plume flow fields consider two-phase effects. The analysis of the current SRM nozzle flow field was performed using the Lockheed-Huntsville RAMP Two-Phase Flow program (Ref. 3). The RAMP code allows momentum and energy exchange between the particulate and gaseous phases, thus allowing the particles to affect the nozzle and exhaust plume expansion. The supersonic RAMP solution was initiated using a start-line generated by Kliegel's transonic program (Ref. 4).

The sensitivity study was conducted by parametrically perturbing various input parameters to the flowfield solution about a nominal set of conditions. Nominal conditions were chosen to be:

- Nozzle area ratio, $A/A^* = 7.16$
- Nozzle throat radius of curvature, $R_e/R_t = 2.0$
- Nozzle throat inlet angle, $\theta_I = 30$ deg
- Nozzle lip half angle, $\theta_{lip} = 11.202$ deg
- Nozzle throat radius, $R_t = 2.2679$ feet
- Chamber pressure, $P_c = 700$ psia
- Constant gaseous thermodynamic properties

  $\gamma = 1.25$

  $M_w = 20.245$

3

• Particles

loading, $\dot{\omega}_p/\dot{\omega}_g = 0.4$

mean particle size, $r_p = 6.0$ microns

drag coefficient - Kliegel (Ref. 8)

heat transfer coefficient = Drake (Ref. 10)

$C_{P_L} = 0.3395$ Btu/lbm-$^\circ$R

$C_{P_S} = 0.2676$ Btu/lbm-$^\circ$R

$H_{P_L} = 1612.1$ Btu/lbm

$H_{P_S} = 1112.8$ Btu/lbm

The nozzle flow field for these sets of nominal values provided a reference set of exit properties and consequently δ_j as a function of expansion pressure ratio. The sensitivity of δ_j to change in the input data was then obtained by parametrically varying the input data about the nominal conditions and examming the change in δ_j.

Frozen and equilibrium gas thermochemistry models were used as comparative models. Data for these models were obtained using a version of TRAN72 (Ref. 5) which has been modified (Ref. 6) to meet the requirements of the RAMP Two-Phase Flow program. The tables of thermodynamic and transport properties were constructed such that variations in gas properties due to changes in total enthalpy, entropy and temperature are considered.

An important parameter for a two-phase calculation is the particle size distribution. For a nominal SRM condition a mass mean radius of 6 microns was used. This was obtained based on a mean diameter versus nozzle throat diameter correlation by Delaney (Ref. 7). For comparison, calculations were also performed using the particle size distribution in Table 1. The ratio of particle mass to total propellant mass was nominally selected as 0.4

For the purposes of this document, a variation in δ_j of less than one degree is considered minimal and a variation in δ_j greater than two degrees

4

is considered significant. With the current Space Shuttle configuration, a one degree change in δ_j results in a change of 100 lbs in allowable payload weight (Ref. 7).

2.2 CHAMBER PRESSURE EFFECT

To investigate the effect of chamber pressure on the initial plume expansion angle, δ_j, RAMP nozzle calculations were generated for chamber pressures of 500, 600, 700, 800 and 900 psia. A figure was constructed with chamber to ambient pressure ratio plotted as a function of δ_j for each chamber pressure, In Fig. 1 it is evident that chamber pressure has a minimal effect on δ_j with a maximum variation of approximately one degree.

2.3 EFFECT OF GAS THERMOCHEMISTRY MODEL

The RAMP code has the capability to use several gas thermodynamic and transport property models. The nominal model chosen for this analysis is one in which the thermodynamic (γ, molecular weight) and transport properties (except viscosity) are held constant. The equilibrium thermochemistry model uses tabulated data from the TRAN72 code and allows thermodynamic properties to vary with changes in total enthalpy, entropy and temperature. The frozen thermochemistry model uses tabulated thermodynamic properties but assumes that no chemical reactions occur after the flow has expanded beyond a static to total pressure ratio specified by the user. The frozen chemistry model used in this analysis assumed that chemical reactions ceased at the nozzle throat. Nozzle calculations were performed with each chemistry model for a chamber pressure of 700 psia exhausting to ambient pressures ranging from 15.21 to 0.07 psia.

In Fig. 2, chamber to ambient pressure ratio is plotted as a function of δ_j for each chemistry model. For chamber to ambient pressure ratios less than 400, the use of different chemistry models did not produce any significant deviations in δ_j. At higher chamber to ambient pressure ratios, P_c/P_∞, the chemically frozen and equilibrium chemistry models produced significantly

different values for δ_j. For a pressure ratio, P_c/P_∞, of 10,000, the difference in δ_j using the different chemistry models was 4 degrees. At high pressure ratios the constant thermodynamic property model typically produced a δ_j approximately one degree greater than the δ_j produced by the chemically frozen model. Above a pressure ratio of 1000, δ_j values calculated with the constant property model deviate significantly from the δ_j values calculated with the equilibrium model. The difference in initial plume expansion for these models at $P_c/P_\infty = 10,000$ is 3 degrees. The difference in γ among the three models investigated appears to be the parameter which produces the variations in δ_j illustrated in Fig. 2.

Nozzle calculations were performed to investigate the effect on δ_j of the value of γ assumed in the constant thermodynamic property model. Calculations were generated using values for γ of 1.250 and 1.179. It is evident in Fig. 3 that the effect on δ_j is significant. The difference in δ_j for the two values of γ is 1 degree at $P_c/P_\infty = 100$ and 7 degrees at $P_c/P_\infty = 10,000$. A lower value for γ produces a higher initial expansion angle. This trend is confirmed in Fig. 2 where the equilibrium chemistry model had the lowest exit plane γ of the three models and produced the highest initial expansion angles.

2.4 NOZZLE GEOMETRY EFFECT

Initial plume expansion angle sensitivity to two parameters defining nozzle geometry was investigated. The parameters were nozzle throat radius of curvature ratio and nozzle inlet angle. The nozzle inlet angle directly effects the structure of the subsonic and transonic portions of the nozzle flow field and the supersonic startline generated by the Kliegel transonic code. The startline characteristics subsequently impact the supersonic expansion.

Nozzle radius of curvature ratio and inlet angle were varied since the Kliegel transonic solution will not handle radius of curvature ratios below about 1.5 nor inlet angles greater than 45 deg. Therefore, to run two-phase solutions for nozzles whose geometries do not fall within the Kliegel capability the throat geometry must be modified. For this reason nozzle geometric effects on δ_j were examined.

6

Nozzle configurations with nozzle throat radius of curvature ratios of 1.5, 1.75, 2.0, 2.25 and 2.50 were input to the RAMP code and nozzle flow fields calculated with a chamber pressure of 700 psia exhausting to various ambient pressures. A figure was constructed with chamber to ambient pressure ratio plotted as a function of δ_j for each throat radius of curvature ratio. In Fig. 4 the variation of δ_j with throat radius of curvature ratio is 0.5 degrees or less over the entire pressure ratio range. Throat radius of curvature ratio has a minimal effect on the initial plume expansion.

Figures 5 and 6 are figures depicting the deviation δ_j with throat inlet angle for a range of operating pressure ratios. The data presented in Fig. 5 were calculated using one mean particle size (6 micron radius). The data in Fig. 6 were calculated using the particle size distribution of Table 1. Variation of the throat inlet angle from 20 to 45 degrees resulted in a δ_j variation of 0.5 to 1.0 degree at the higher pressure ratios and less than 0.5 degree at pressure ratios less than 100. These data are presented in the nomographs of Figs. 5 and 6. For the calculations using one mean particle size, δ_j was highest at a given pressure ratio for an inlet angle of 20 degrees. For the calculations using a particle size distribution, δ_j was highest at a given pressure ratio for an inlet angle of 30 degrees. The variation of δ_j with throat inlet angle was considered minimal.

2.5 PROPELLANT LOADING EFFECT

The weight percent of solid particles in a propellant has significant effects on the nozzle and exhaust plume expansion of a solid propellant motor. To assess the sensitivity of δ_j to particle propellant loading ($\dot{\omega}_p/\dot{\omega}_g$), nozzle flow fields were calculated for a range of propellant loadings ($\dot{\omega}_p/\dot{\omega}_g$ = 0.3 to 0.5) and chamber to ambient pressure ratios. The parametric calculations were generated using two chemistry models, the constant thermodynamic property model and the chemically frozen model. The figure in Fig. 7 indicates that at low pressure ratios the variation of δ_j with $\dot{\omega}_p/\dot{\omega}_g$ is less than 0.5 degree. However, as the pressure ratio is increased the variation of δ_j with $\dot{\omega}_p/\dot{\omega}_g$ increases to a significant level, e.g., a 2 degree variance at a pressure ratio of 6000 between calculations with a $\dot{\omega}_p/\dot{\omega}_g$ = 0.3

7

and calculations with a $\dot{\omega}_p/\dot{\omega}_g = 0.5$. As $\dot{\omega}_p/\dot{\omega}_g$ increases for a given pressure ratio, the greater the initial plume expansion.

Results are presented in Fig. 8 for calculations using the chemically frozen thermochemistry model. Variations in δ_j with $\dot{\omega}_p/\dot{\omega}_g$ increased with increasing chamber to ambient pressure ratio. For a given pressure ratio the initial plume expansion angle increases with increasing $\dot{\omega}_p/\dot{\omega}_g$. This effect is the result of the coupling between the gaseous and particulate phases which results in a higher exit pressure as particle propellant loading is increased. The higher exit pressure requires a greater initial plume expansion to expand to the same ambient pressure.

2.6   EFFECT OF MEAN PARTICLE SIZE

An important input parameter to the analytical RAMP flowfield calculations is mean particle size. The particle drag and heat transfer coefficients vary with the square of the spherical particle radius. Thus, the temperature and velocity lags between the gas and particle phases is a strong function of particle size. To investigate the deviation of δ_j with different values for this empirically determined parameter, nozzle analyses were generated with various mean particle sizes. Comparative calculations were also made to investigate the effect of assuming one mean particle size as opposed to assuming a distribution of particle sizes about the given mean size.

In Fig. 9, chamber to ambient pressure ratio is plotted as a function of δ_j for a calculation assuming a mean particle size versus a calculation assuming a distribution of particle sizes (Table 1). There was no difference in δ_j for a given pressure ratio between calculations using the different particle size assumptions.

The results of nozzle calculations using different mean particle sizes (r_{mp} = 4 - 8 microns) are presented in Fig. 10. At a given pressure ratio, the initial plume expansion angle decreased for increasing mean particle

size. The difference δ_j for r_{mp} = 4 and for r_{mp} = 8 was approximately 2 degrees across the entire range of pressure ratios. Thus, there is a significant variation in δ_j with the empirically determined mean particle size.

2.7 EFFECT OF MEAN PARTICLE SIZE FOR DIFFERENT VALUES OF LOCAL DRAG COEFFICIENT

Two empirically derived constants which are impacted by mean particle size and have a significant effect on the coupling between the gas and particle phases are the heat transfer coefficient and the local drag coefficient. An analysis was performed to determine the sensitivity of δ_j to different mean particle sizes and different heat transfer and drag coefficients. The nominal local drag coefficient used in calculating the results (presented in Fig. 10) was doubled and halved and used in nozzle calculations in which mean particle size and pressure ratio were parametrically varied. The results are presented in Figs. 11 and 12, respectively. Figure 11 represents the results obtained with a drag coefficient double the nominal local drag coefficient. For chamber to ambient pressure ratios less than 700, results were similar to those obtained with the nominal value of drag coefficient. The intial expansion angle decreased with increasing mean particle size at a given pressure ratio. However, above a pressure ratio of 700 δ_j increased with increasing mean particle size. Differences in δ_j values ranged from 0 to 2 degrees at pressure ratios below 700 and from 0 to 1 degree above 700. Figure 12 represents the results obtained with a drag coefficient of one half the nominal drag coefficient. For all values of chamber to ambient pressure ratio, results were qualitatively identical to those obtained with the nominal value of drag coefficient. The initial expansion angle decreased with increasing mean particle size at a given pressure ratio. Quantitatively, the variation of δ_j with mean particle size was greater for calculations using a value of one half the nominal drag coefficient than for calculations using the nominal value. For a deviation in mean particle radius from r_{mp} = 4 to r_{mp} = 8, the maximum variation in δ_j was approximately 3 degrees.

9

A value of local drag coefficient of twice the nominal value resulted in quantitatively smaller variations in δ_j than calculations using the nominal drag coefficient. Calculations using a drag coefficient one half the nominal value resulted in quantitatively larger variations in δ_j with mean particle size than calculations using the nominal drag coefficient.

2.8 EFFECT OF MEAN PARTICLE SIZE FOR DIFFERENT VALUES OF LOCAL HEAT TRANSFER COEFFICIENT

The nominal local heat transfer coefficient used in calculating the results presented in Fig. 10 was doubled and halved and used in nozzle calculations in which mean particle size and pressure ratio were parametrically varied. The results are contained in the nomographs of Figs. 13 and 14, respectively. Figure 13 represents the results obtained with a local heat transfer coefficient double the value of the nominal heat transfer coefficient. For chamber to ambient pressure ratios greater than 700, results were similar to those obtained with the nominal value of heat transfer coefficient. The initial expansion angle decreased with increasing mean particle size at a given pressure ratio. The variation in δ_j with mean particle size was negligible at a chamber to ambient pressure ratio of 700. However, below a pressure ratio of 700 δ_j increased with increasing mean particle size. Differences in δ_j values for various mean particle sizes varied from 0 to 0.5 degrees across the entire pressure ratio range.

Figure 14 represents the results obtained with a local heat transfer coefficient of one-half the value of the nominal heat transfer coefficient. For all values of chamber to ambient pressure ratio, results were qualitatively identical to those obtained with the nominal value of heat transfer coefficient. The initial expansion angle decreased with increasing mean particle size at a given pressure ratio. Quantitatively, the variation in δ_j with mean particle size was greater for calculations using the value of one-half the nominal heat transfer coefficient than the calculations using the nominal heat transfer coefficient. For a variation in mean particle radius from $r_{mp} = 4$ to $r_{mp} = 8$, the maximum deviation in δ_j was approximately 2

10

degrees for calculations using values of one-half the nominal heat transfer coefficient.

2.9   EFFECT OF DRAG COEFFICIENT MODEL

Several empirical models are currently in use for calculating particle drag coefficients. The models were developed by Kliegel (Ref. 8) and Crowe (Ref. 9), respectively. An analysis was conducted to assess the sensitivity of δ_j to different drag coefficient models. In Fig. 15 chamber to ambient pressure ratio is plotted as a function of δ_j for calculations using drag coefficient models developed by Kliegel and Crowe. There was no difference in δ_j at a given pressure ratio for calculations using different drag coefficient models. These calculations were performed assuming a mean particle size with r_{mp} = 6 microns.

An analysis was conducted to investigate the sensitivity of δ_j to different values of drag coefficient. Using the Kliegel drag model and parametrically varying pressure ratio, nozzle calculations were generated using different values of drag coefficient (0.5 x Kliegel C_D to 2.0 x Kliegel C_D). The results of these calculations are represented by the nomograph of Fig. 16. For a given pressure ratio, the initial plume expansion angle increases slightly for increasing values of drag coefficient. Over the range of pressure ratios investigated, the maximum variation in δ_j was less than one degree. The increased initial plume expansion angle with increased value of drag coefficient resulted from the coupling between the gas and particulate phases. The increased particle drag coefficient increased the momentum loss of the gas resulting in a lower gas velocity and higher pressure at the nozzle exit plane. The higher exit pressure produced a greater initial plume expansion. The change in δ_j with the value of drag coefficient (assuming a mean particle size) was minimal over the range of drag coefficient values considered.

The sensitivity of δ_j to different drag coefficient models assuming a distribution of particle sizes was investigated. The distribution of particle sizes in Table 1 was used in nozzle calculations with drag coefficient models

11

by Kliegel and Crowe. In Fig. 17 chamber to ambient pressure ratio is plotted as a function of δ_j for calculations using different drag coefficient models. At a given pressure ratio, there was no difference in δ_j for nozzle calculations using different drag coefficient models.

An analysis was conducted to investigate the sensitivity of δ_j to different values of drag coefficient using a distribution of particle sizes. Using the Kliegel drag model and parametrically varying pressure ratio, nozzle calculations were generated using different values of drag coefficient (0.5 x Kliegel C_D to 2.0 x Kliegel C_D). The results of these calculations are presented in Fig. 18. Across the range of pressure ratios investigated, the initial plume expansion angle increased with increasing drag coefficient. As pressure ratio increased, the difference in δ_j for calculations using various values of C_D increased. Quantitatively, for the range of drag coefficients used, the maximum deviation in δ_j at given pressure ratio was approximately one degree. The quantitative and qualitative results were the same as the results obtained from calculations which assumed a mean particle size. Changes in δ_j with values of local drag coefficient were considered minimal.

2.10   EFFECT OF VALUE OF HEAT TRANSFER COEFFICIENT

Nozzle calculations were generated to assess the effect of the value of heat transfer coefficient on the initial plume expansion angle. Pressure ratio was parametrically varied for calculations using values of the local heat transfer coefficient ranging from 0.5 x Drake $\dot{Q}$ to 2.0 x Drake $\dot{Q}$. In Fig. 19, the variation of δ_j with heat transfer coefficient at a given pressure ratio is illustrated. The initial plume expansion angle increases with increasing local heat transfer coefficient for a given chamber to ambient pressure ratio. For the range of pressure ratios and heat transfer coefficients investigated, difference in δ_j at a given pressure ratio ranged from 0.5 to 1.0 degree.

To investigate the combined effect of heat transfer coefficient and thermochemistry model, parametric calculations were performed assuming the flow to be chemically frozen at the nozzle throat. The value of the local heat transfer coefficient was varied from 0.5 x Drake $\dot{Q}$ to 2.0 x Drake $\dot{Q}$. The results of the calculations are presented in Fig. 20. For a given pressure ratio, δ_j increases with increasing value of heat transfer coefficient. The maximum deviation in δ_j at a given pressure ratio was 2.5 degrees. Typically, the variation in δ_j was greater in the calculations using the chemically frozen thermochemical model than in the nominal calculations assuming constant thermodynamic properties.

To investigate the combined effect of heat transfer coefficient and particle size distribution, parametric calculations were performed assuming the particle size distribution of Table 1 rather than the nominal mean particle radius of 6 microns. As in the previous cases, the value of the local heat transfer coefficient was varied from 0.5 x Drake $\dot{Q}$ to 2.0 x Drake $\dot{Q}$. Qualitatively and quantitatively the results presented in Fig. 21 are similar to those in Fig. 19 obtained with a mean particle radius of 6 microns. At a given chamber to ambient pressure ratio, δ_j increased with increasing heat transfer coefficient. The variation of δ_j with heat transfer coefficient over the range of pressure ratios was approximately 0.5 to 1.0 degree. It was concluded that the differences in particle size distributions investigated did not affect the variation of δ_j with heat transfer coefficient.

2.11 COMBINED EFFECT OF PARTICLE DRAG AND HEAT TRANSFER COEFFICIENT

The sensitivity of δ_j to simultaneous changes in local drag and heat transfer coefficients was investigated. Nozzle calculations were performed with; (1) a local drag coefficient of twice the Kliegel drag coefficient and a local heat transfer coefficient of twice the Drake heat transfer coefficient (case 1), (2) a nominal heat transfer coefficient and a drag coefficient of one-half the Kliegel coefficient (case 2), (3) a nominal drag coefficient and a heat transfer coefficient of one-half the Drake coefficient (case 3).

13

Results of these calculations are plotted comparatively in Figs. 22 through 25. In Fig. 22 the parametric variation of δ_j with pressure ratio for cases 1 and 3 is plotted along with the results of calculations using nominal values. Over most of the pressure ratio range, the nominal curve fell between the curves for calculations using one-half the Drake heat transfer coefficient and for calculations using twice the value of the Kliegel drag and Drake heat transfer coefficients. The maximum difference in δ_j for the two later curves was approximately two degrees. The results of calculations for cases 1 and 2 and nominal conditions are presented in Fig. 23. There was no difference in values of δ_j at a given pressure ratio for the nominal curve and the curve generated with one-half the value of the local drag coefficient. This result is verified by results presented in Fig. 16. At pressure ratios below 500, the curves for all three cases coincided. Above a pressure ratio of 500, calculations using drag and heat transfer coefficients twice the nominal values diverged from the nominal curve. At a given pressure ratio above 500, the initial plume expansion was greater for calculations using twice the nominal drag and heat transfer coefficients. This trend agrees qualitatively with the results presented in Figs. 16 and 19 in which the drag and heat transfer coefficients, respectively, were increased separately.

Figure 24 compares the results of three calculations: (1) using a nominal value of heat transfer coefficient and a drag coefficient of twice the nominal value; (2) using twice the nominal values of heat and drag coefficients; and (3) using nominal values. The curves of chamber-to-ambient pressure ratio as a function of δ_j for all three conditions coincide at pressure ratios below 500. Above a pressure ratio of 500, the curves for the off-nominal conditions diverged from the curve generated with nominal values for drag and heat transfer coefficients. Both curves generated with twice the nominal value of drag coefficient coincided over the entire pressure ratio range investigated. Thus the drag coefficient appeared to be a stronger driving function of δ_j than the heat transfer coefficient. Qualitatively, the trends are similar to the results presented in Figs. 16 and 19 in which heat transfer and drag coefficients

14

were increased and produced larger δ_j values at a given pressure ratio. Above a pressure ratio of 500, calculations using values of drag and heat transfer coefficients of twice the nominal values produced δ_j values of up to 1 degree greater at a given pressure ratio than calculations using the nominal values. The maximum difference in δ_j (1 degree) between nominal and off-nominal calculations (assuming values of heat transfer and drag coefficients twice the nominal values) was the same order of magnitude as the difference in δ_j between nominal calculations and calculations generated with the coefficients doubled separately (Figs. 16 and 19).

15

Section 3
CONCLUSIONS

The sensitivity of the initial plume expansion to various operating and input parameters was investigated. The variation of δ_j with changes in chamber pressure at constant pressure ratio was minimal. At low chamber-to ambient pressure ratios, the use of different chemistry models did not produce any variation in δ_j. The difference in γ among the three chemistry models resulted in large difference in δ_j at the high pressure ratios. The largest difference in δ_j at a given pressure ratio occurred between calculations using a constant property model and calculations using an equilibrium chemistry model. Large differences in δ_j (7 degrees) were obtained when different values of γ were used in calculations with a constant property chemistry model. At a given pressure ratio, as γ decreases the initial expansion angle, δ_j, increases. Changes in nozzle throat radius of curvature ratio and nozzle inlet produced minimal changes in δ_j. At pressure ratios above 1000, propellant particle loading produced significant differences in δ_j. The initial plume expansion angle increased with increasing propellant loading at a given pressure ratio. There was no difference in δ_j between calculations assuming a mean particle size and calculations assuming a particle size distribution. As mean particle size was varied from $r_{mp} = 4$ to $r_{mp} = 8$, the initial plume expansion angle decreased by 2 degrees. The assumed mean particle size thus has a significant effect on δ_j. There was no difference in δ_j at a given pressure ratio for calculations using different drag coefficient models, e.g., Kliegel and Crowe. Parametric variation of local drag coefficient from 0.5 x Kliegel C_D to 2.0 x Kliegel C_D produced a maximum δ_j variation of less than one degree. The parametric variation of heat transfer coefficient indicated increasing δ_j with increasing values of local heat transfer coefficient. The deviation of δ_j with heat transfer coefficient was considered minimal. The effect on initial plume expansion angle from combined changes in local drag and heat transfer coefficients

16

was investigated. Qualitatively and quantitatively, the results were similar to those obtained in calculations in which only one of the coefficients was changed at a time. It was concluded that the coupling between the drag and heat transfer calculations was minimal.

In summary the following qualitative effects on initial plume expansion were observed for each parameter:

- Chamber pressure — minimal effect
- Chemistry model — large variation in δ_j
- Nozzle throat radius of curvature ratio and throat inlet angle — minimal effect
- Mean particle size assumption versus particle distribution assumption — no effect
- Mean particle size — large variations in δ_j
- Propellant particle loading $(\dot{\omega}_p/\dot{\omega}_g)$ — significant variations in δ_j
- Drag coefficient model (Kliegel versus Crowe) — no effect
- Drag coefficient value — minimal effect
- Heat transfer coefficient value — minimal effect
- Combined changes in value of drag and heat transfer coefficients — minimal effect.

REFERENCES

1. Stone, J. S., "Development of Launch Vehicle Five Full Scale Base Drag from Wind Tunnel Plume Test Data," Internal Letter No. SAS/AERO/75-097, Rockwell International, Downey, Calif., February 1975.

2. Sims, J. L., "Plume Technology Program -- Base Pressure Correlation," Plume Simulation Conference, Marshall Space Flight Center, Ala., February 1974.

3. Penny, M. M., S. D. Smith, L. R. Baker and R. J. Prozan, "Two-Phase Flow Development," LMSC-HREC TR D390040, Lockheed Missiles & Space Company, Huntsville, Ala., January 1974.

4. Kliegel, J. R. and G. R. Nickerson, "Axisymmetric Two-Phase Gas Performance Program — Vol. I," NASA CR 92069, April 1967.

5. Gordon, S., and Bonnie J. McBride, "Computer Program for Calculation of Complex Chemical Equilibrium Compositions, Rocket Performance, Incident and Reflected Shocks and Chapman-Jouquet Detonations," SP-273, NASA-Lewis Research Center, Cleveland, Ohio, 1971.

6. Sulyma, P. R., and L. R. Baker, "User's Guide for TRAN72 Computer Code Modified for Use With RAMP and VOFMOC Flowfield Codes," LMSC-HREC TM D390409, Lockheed Missiles & Space Company, Huntsville, Ala., October 1974.

7. Roberts, B. B., "Minutes for Meeting of Ad Hoc Working Group on Plume Simulation," Johnson Space Flight Center memo EX 32/7506-106, Houston, Texas, May 1975.

8. Delaney, Lawrence J., "Particle Characteristics in Two-Phase Plumes," Martin Marietta Corporation, Friendship International Airport, Md.

9. Kliegel, J. R., "Gas Particle Nozzle Flows," Ninth Symposium on Combustion, Academic Press, New York, 1963.

10. Crowe, C. J. "Drag Coefficient of Particles in a Rocket Nozzle," AIAA J., Vol. 5, No. 5, May 1967.

11. Drake, R. M., "Discussion on G. C. Bliet and G. Leppert: Forced Convection Heat Transfer from an Isothermal Sphere to Water," JANAF Heat Transfer, American Society Mechanical Engineers, Vol. 77, 1955.

Table 1

PARTICLE SIZE DISTRIBUTION

Particle Radius (microns)	Particle Mass Density (lbm/ft^3)	Percentage of Particle Mass Flow Rate
3.15	250	10
4.70	250	20
5.90	250	20
6.95	250	20
8.15	250	20
9.70	250	10

P_c (psia)	P_c/P_e	M_e	T_e
500	33.31	2.62	3254.0
700	33.48	2.03	3258.5
900	32.65	2.61	3268.0

P_c \ P_c/P_∞	60	300	1800	5000
500	20.2	40.9	59.2	67.9
700	20.1	40.9	59.0	67.9
900	20.6	41.4	59.6	67.9

Note: $A/A^* = 7.16$
$\theta_{lip} = 11.202$
$\theta_r = 30$ deg
$r_{mp} = 6\mu$
$\dot{\omega}_p/\dot{\omega}_g = 0.4$
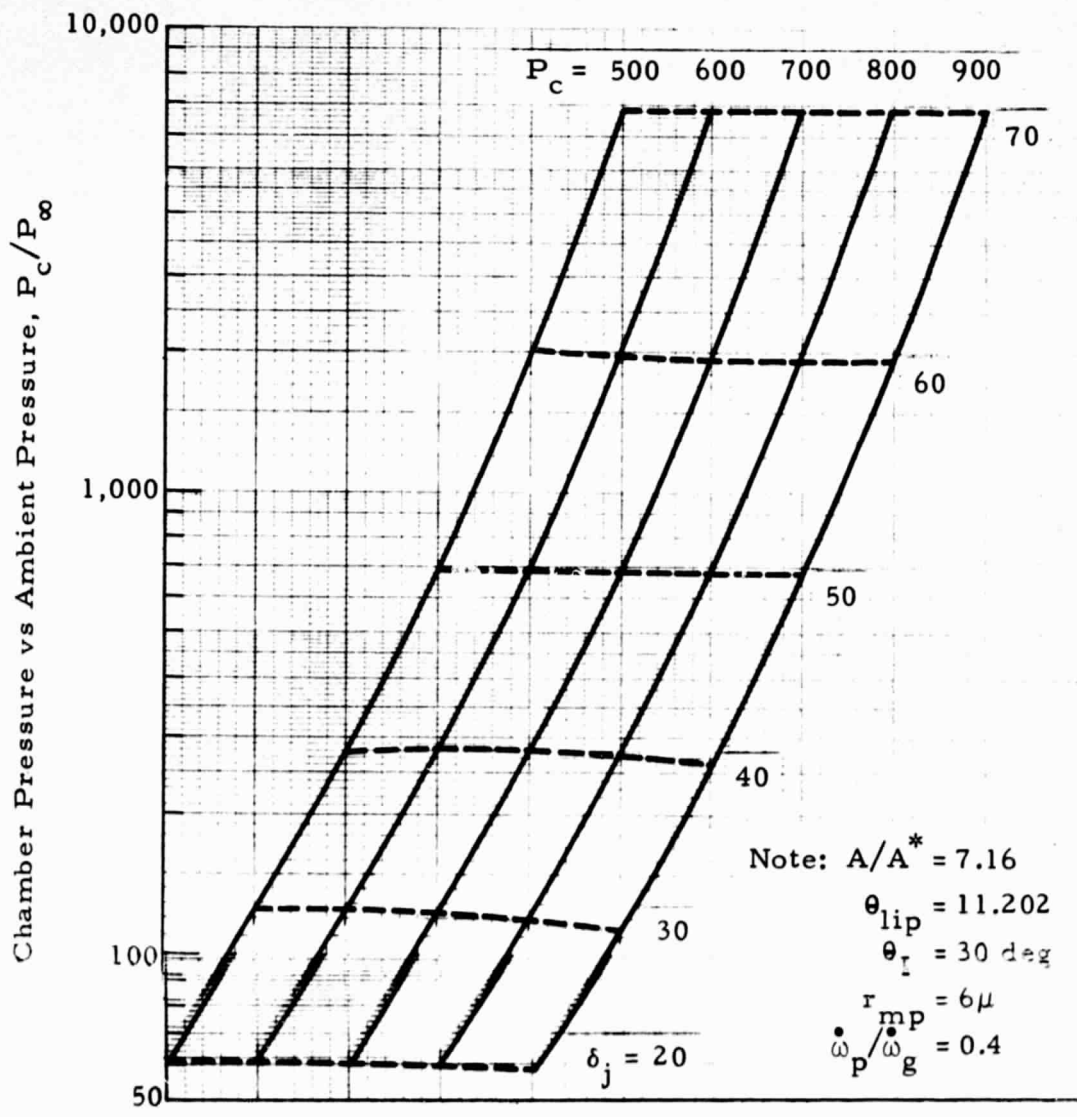
Fig. 1 - Variation of δ_j with Change in Chamber Pressure to Ambient Pressure Ratio

20

LOCKHEED - HUNTSVILLE RESEARCH & ENGINEERING CENTER

Chemistry	P_c/P_e	M_e	T_e	γ_e
Frozen	31.45	2.60	3236.4	1.288
Equilibrium	33.91	2.62	3590.1	1.241
$\gamma = 1.25$, $M_w = 20.245$	33.11	2.62	3258.5	1.250

P_c/P_∞ Chemistry	60	300	1800	5000
Frozen	20.8	40.2	57.1	66.20
Equilibrium	20.0	40.5	59.0	69.15
$\gamma = 1.25$, $M_w = 20.245$	20.4	41.1	59.2	67.80

Symbol	Chemistry Assumption
——————	Chemically Frozen at Throat
– – – – –	Equilibrium Gas Chemistry
— – — – —	$\gamma = 1.25$, $M_w = 20.245$

Note:
P_c = 700 psia
A/A^* = 7.16
θ_{lip} = 11.202 deg
θ_I = 30 deg
R_c/R_t = 2.0
r_{mp} = 6μ
$\dot\omega_p/\dot\omega_g$ = 0.4

Initial Plume Expansion Angle, δ_j (deg)
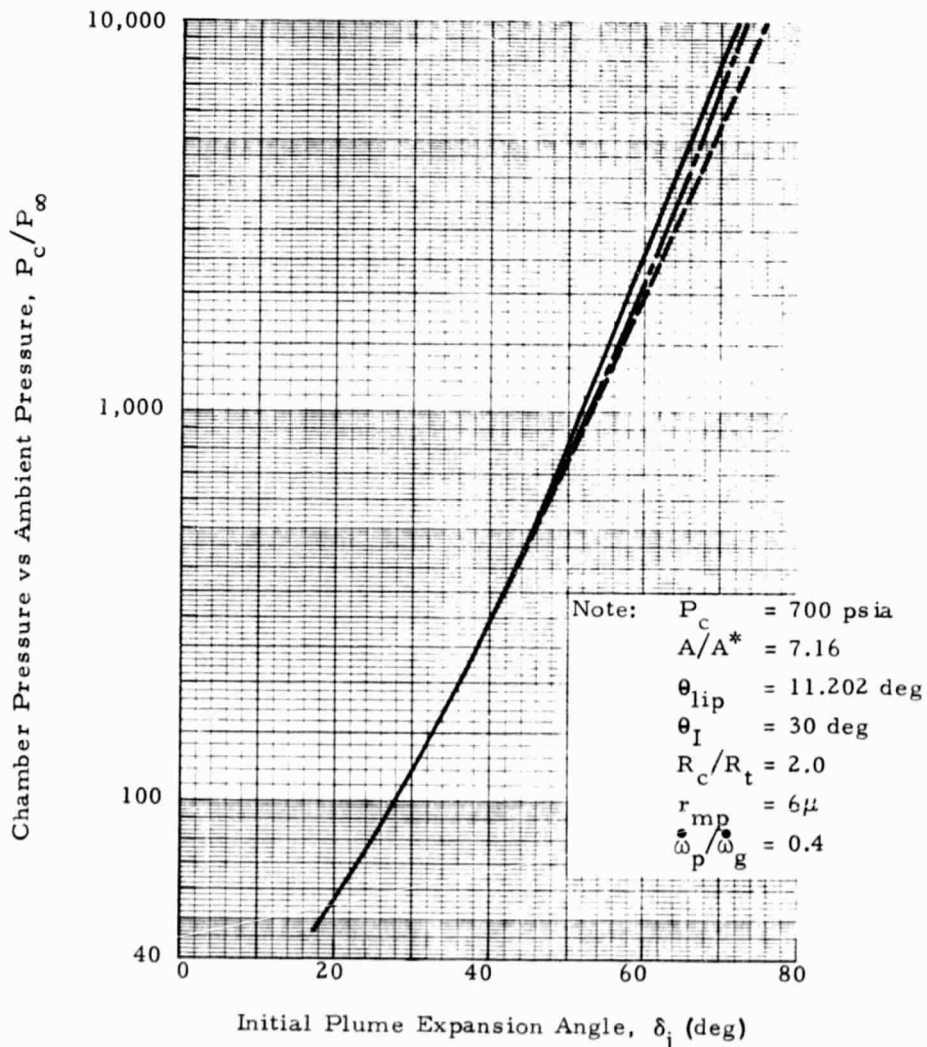
Fig. 2 - Variation of δ_j with Ambient Pressure Ratio for Various Gas Chemistry Assumptions

21

γ	P_c/P_e	M_e	$T_e(^\circ R)$
1.250	32.37	2.61	3282.6
1.179	32.33	2.59	3778.6

Fig. 3 - Variation of δ_j with Ambient Pressure Ratio for Two Values
of γ and a Value of Twice the Local Heat Transfer Coefficient
of Drake

22

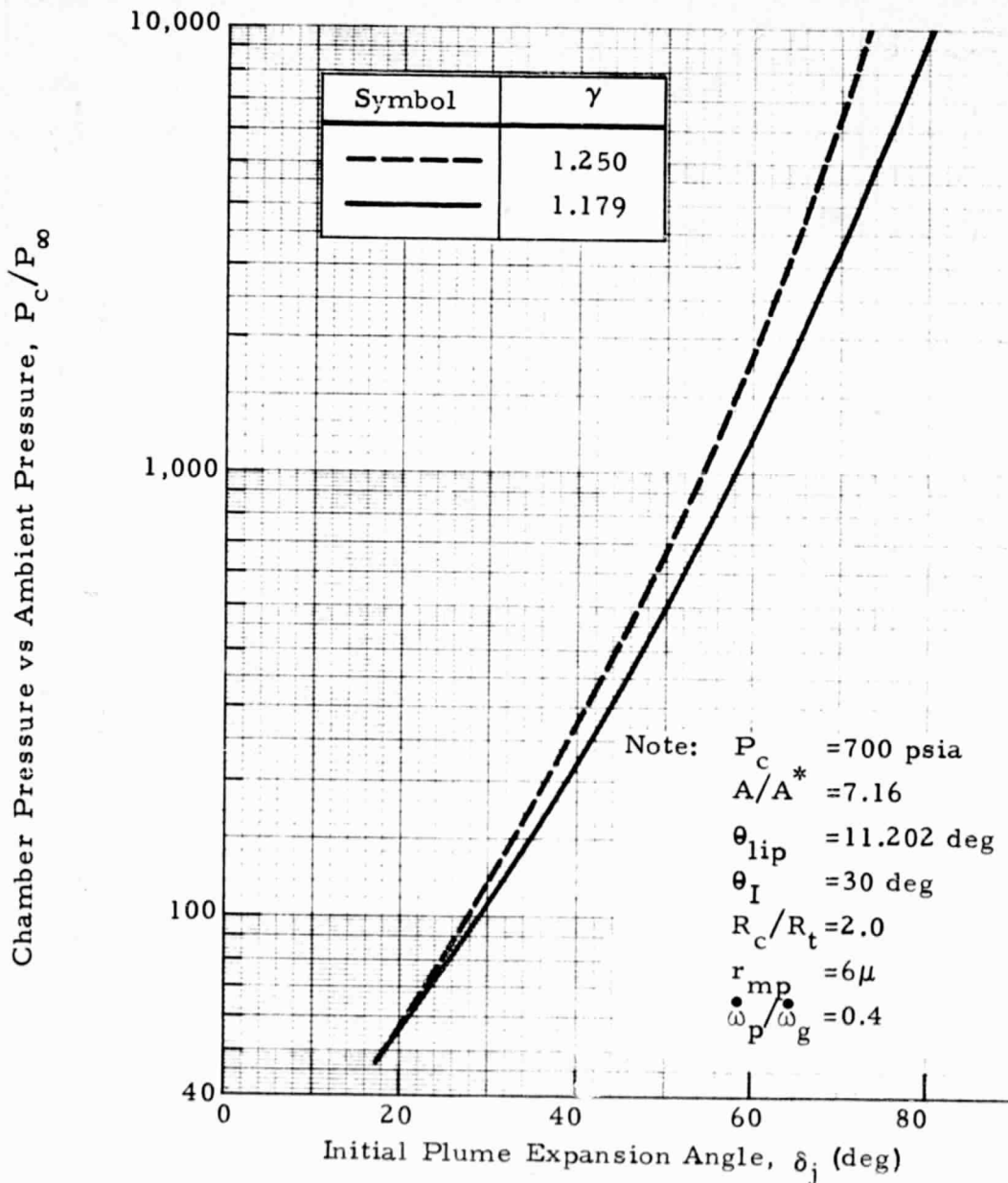| R_e/R_t	P_c/P_e	M_e	$T_e(^oR)$
1.5	32.62	2.62	3262.4
2.0	33.11	2.62	3258.5
2.5	32.98	2.61	3266.3

R_c/R_t $\diagdown$ P_c/P_∞	60	300	1800	5000
1.5	20.5	41.1	59.6	68.9
2.0	20.4	41.1	59.2	67.5
2.5	20.1	41.0	59.3	68.0
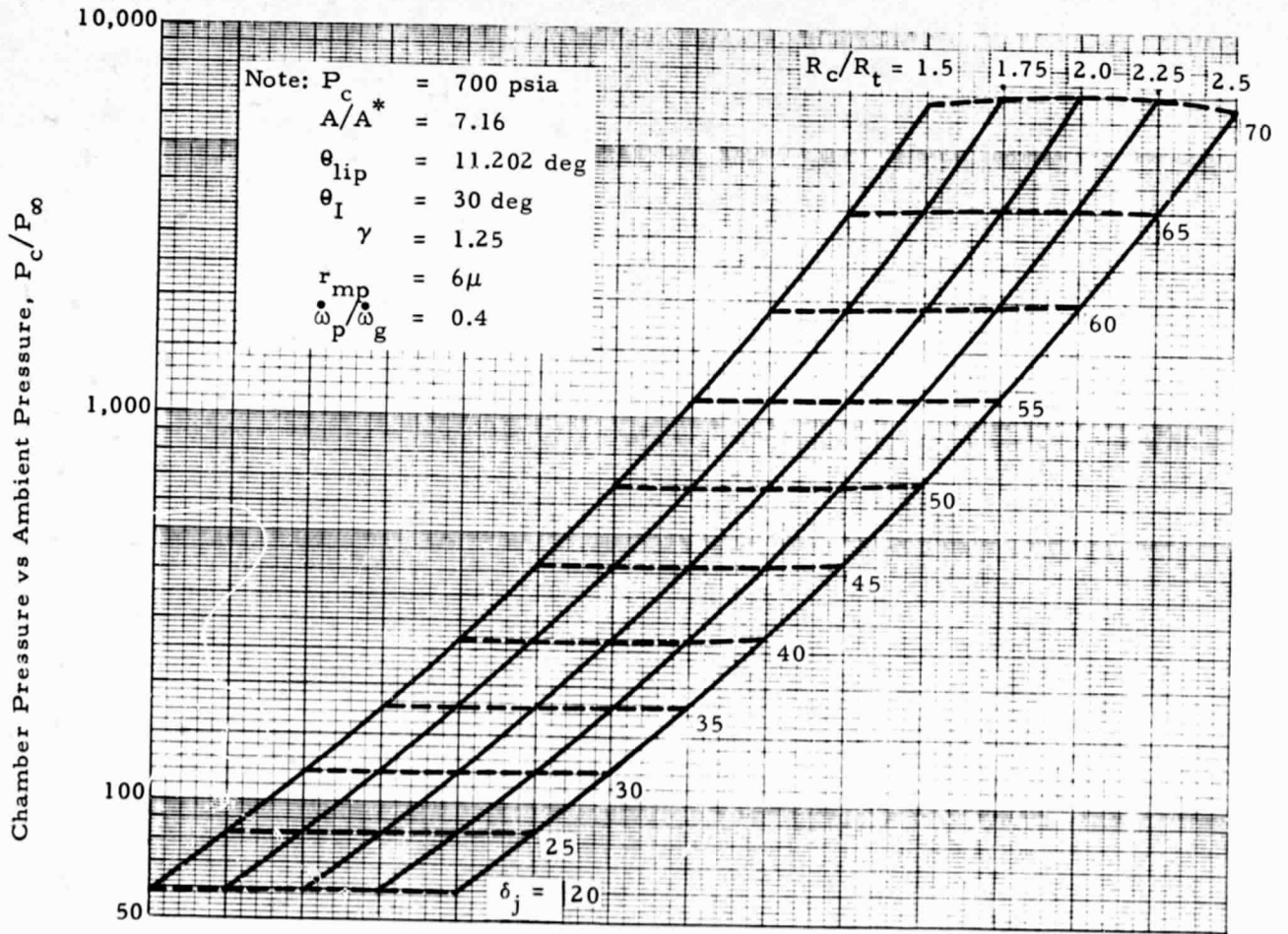
Fig. 4 - Variation of δ_j with Change in Nozzle Throat Radius of Curvature Ratio and Ambient Pressure Ratio

23

θ_I \ P_c/P_∞	60	300	1800	5000
20	20.2	41.1	59.4	67.9
30	20.4	41.1	59.2	67.8
45	19.9	40.6	58.9	67.4

θ_I	P_c/P_e	M_e	$T_e(^oR)$
20	33.02	2.62	3260.3
30	33.11	2.62	3258.5
45	34.00	2.63	3241.2

Note:
$$P_c = 700 \text{ psia}$$
$$A/A^* = 7.16$$
$$\theta_{lip} = 11.202 \text{ deg}$$
$$\theta_I = 30 \text{ deg}$$
$$R_c/R_t = 2.0$$
$$\gamma = 1.25$$
$$r_{mp} = 6\mu$$
$$\dot{\omega}_p/\dot{\omega}_g = 0.4$$
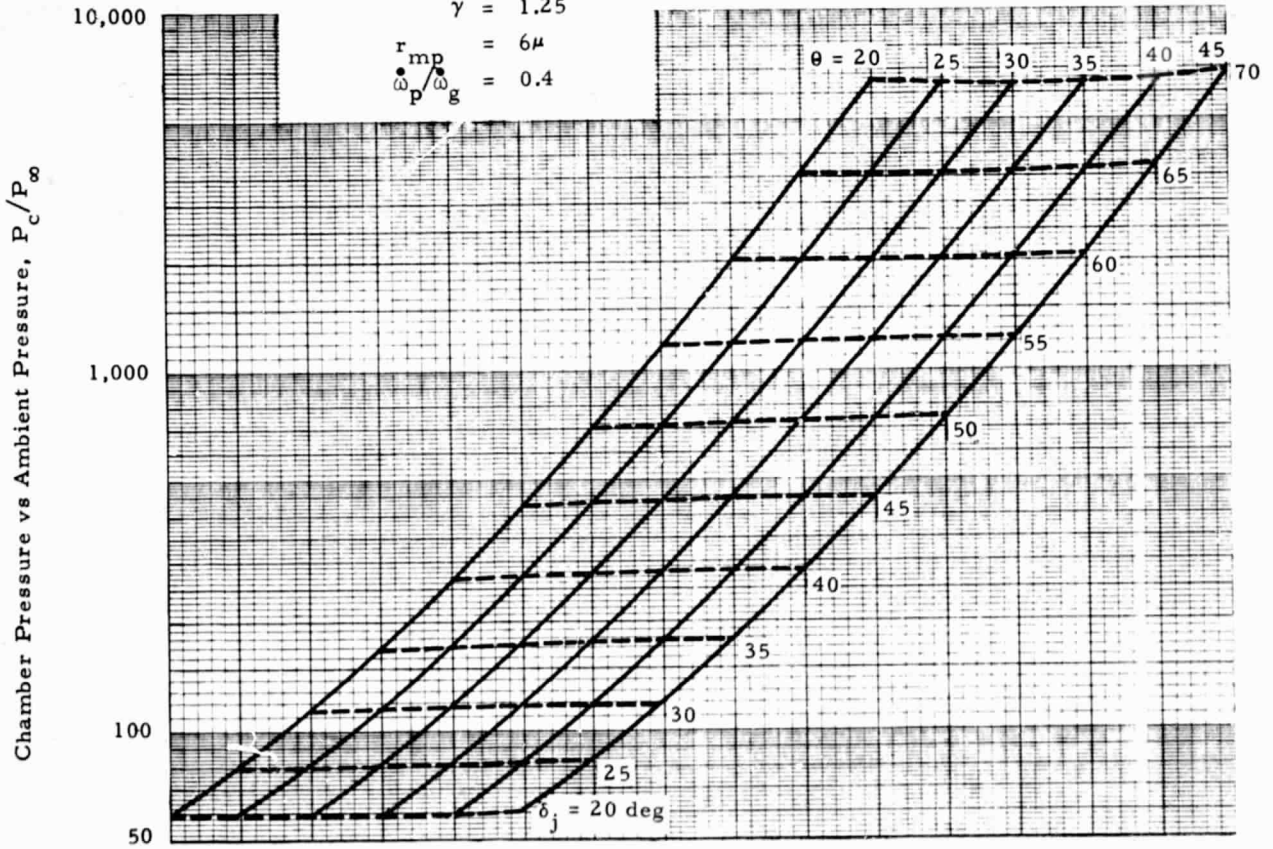
Fig. 5 - Variation of δ_j with Change in P_c/P_∞ and Nozzle Throat Inlet Angle Utilizing a Mean Particle Size

24

θ_I	P_c/P_e	M_e	$T_e(^\circ R)$
20	33.52	2.63	3250.3
30	33.48	2.63	3251.0
45	34.48	2.64	3232.0

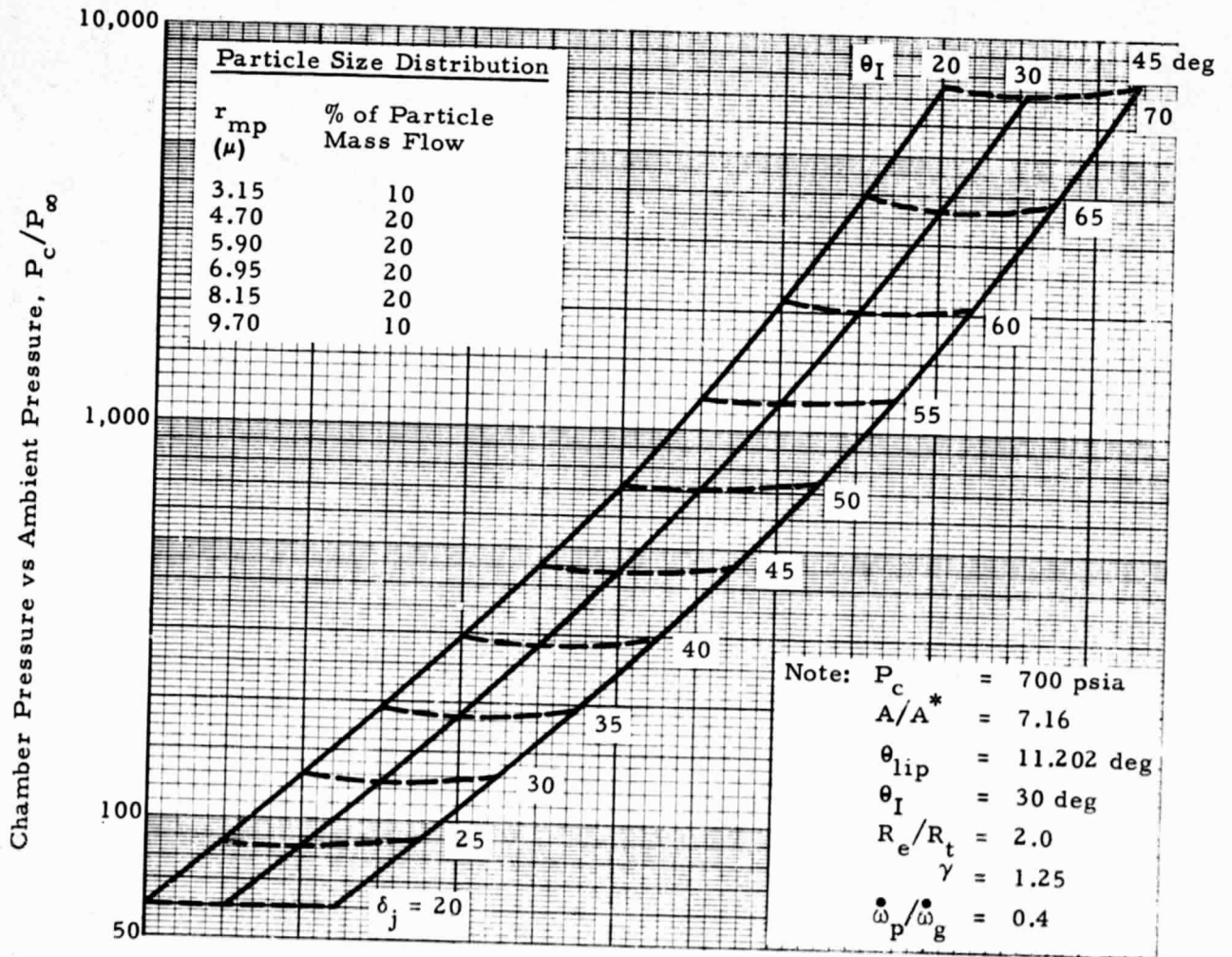| θ_I \ P_c/P_∞	60	300	1800	5000
20	20.1	40.7	58.9	67.5
30	20.1	40.9	59.0	67.7
45	19.7	40.3	58.5	66.9

Fig. 6 - Variation of δ_j with Change in Nozzle Inlet Angle and Ambient Pressure Ratio Assuming a Particle Size Distribution

25

$\dot{\omega}_p/\dot{\omega}_g$ \ P_c/P_∞	60	300	1800	5000
.3	19.6	40	58.2	66.9
.4	20.4	41.1	59.2	67.8
.5	20.8	41.5	60.0	68.9

$\dot{\omega}_p/\dot{\omega}_g$	P_c/P_∞	M_e	$T_e(^\circ R)$
.3	34.02	2.68	3197.9
.4	33.11	2.62	3258.5
.5	32.44	2.57	3309.5

Note: P_c = 700 psia
A/A^* = 7.16
θ_{lip} = 11.202 deg
θ_I = 30 deg
R_c/R_t = 2.0
γ = 1.25
r_{mp} = 6μ
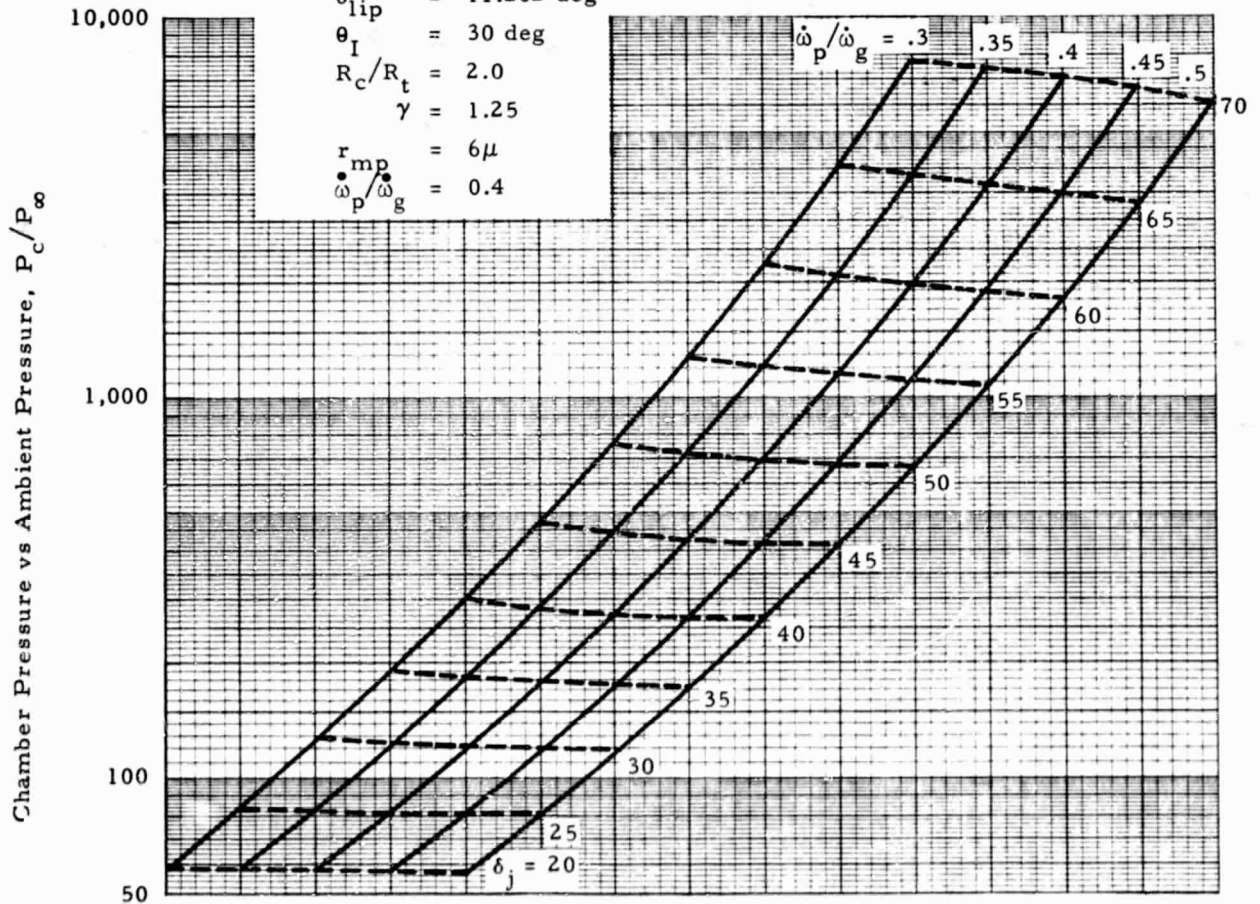$\dot{\omega}_p/\dot{\omega}_g$ = 0.4

Chamber Pressure vs Ambient Pressure, P_c/P_∞

Fig. 7 - Variation of δ_j with Change in Particle Propellant Loading Relative
to the Gas and Ambient Pressure Ratio

26

$\dot{\omega}_p/\dot{\omega}_g$	P_c/P_e	M_e	$T_e(^\circ R)$	γ_e
.3	32.59	2.67	3172.0	1.289
.4	31.45	2.60	3236.4	1.288
.5	30.90	2.56	3282.6	1.287

$\dot{\omega}_p/\dot{\omega}_g$ \ P_c/P_∞	60	300	1800	5000
.3	20.5	39.4	56.0	65.1
.4	20.9	40.2	57.1	66.2
.5	21.1	41.0	58.0	67.3

Note:
P_c = 700 psia
$A/A^* $ = 7.16
θ_{lip} = 11.202 deg
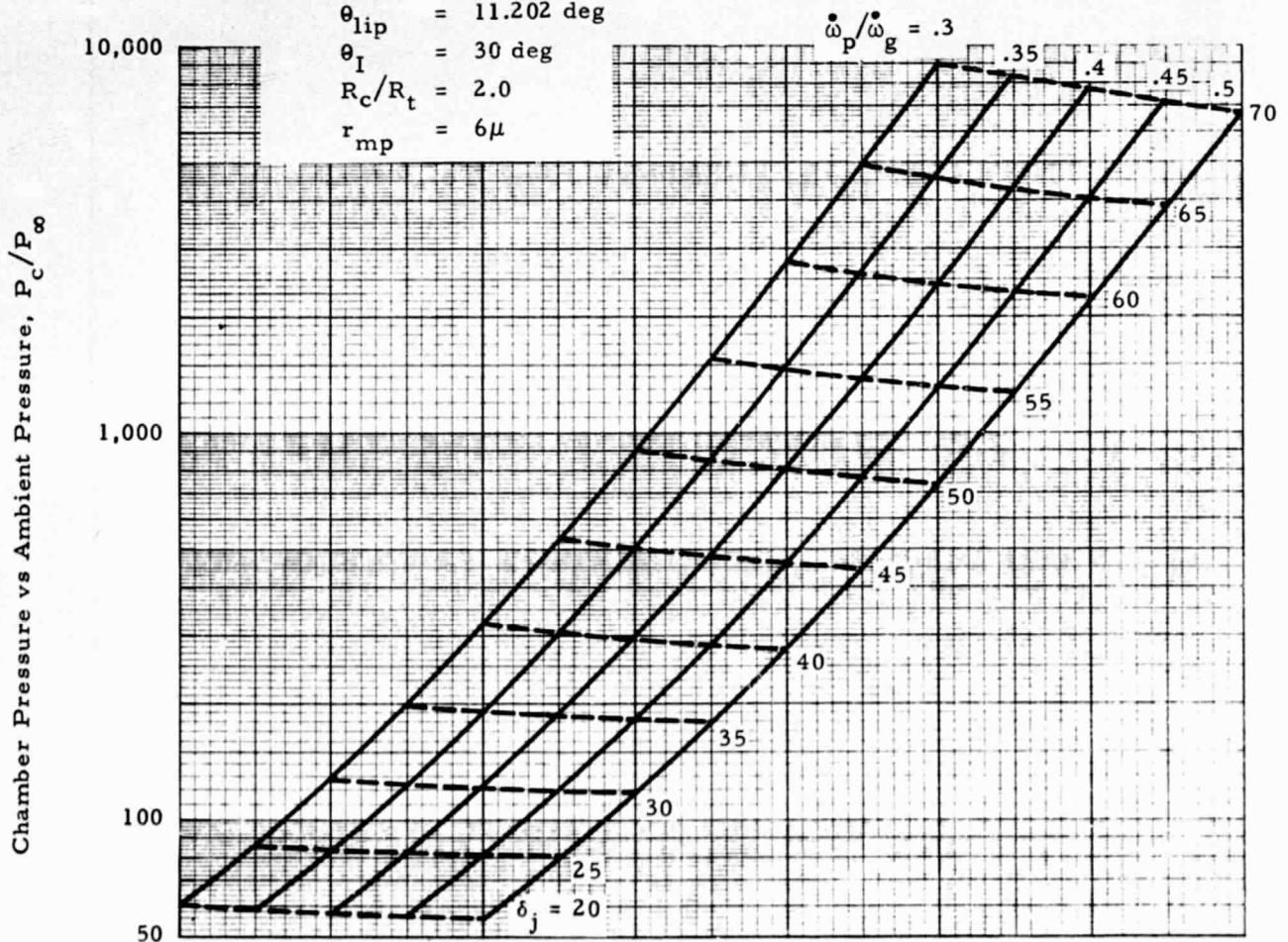θ_I = 30 deg
R_c/R_t = 2.0
r_{mp} = 6μ

Fig. 8 - Variation of δ_j with Change in Particle Loading Relative to the Gas and Ambient Pressure Ratio for the Gas Chemically Frozen at the Throat

27

Symbol	Item
——	Single Particle Size ($r_{mp} = 6\mu$)
✕✕✕	Particle Size Distribution (6μ Mean Size)

Symbol	P_e/P_∞	M_e	$T_e(^oR)$
——	33.11	2.62	3258.5
✕✕✕	33.48	2.63	3251.0

Note:
P_c = 700 psia
A/A^* = 7.16
θ_{lip} = 11.202 deg
θ_I = 30 deg
R_c/R_t = 2.0
γ = 1.25
$\dot\omega_p/\dot\omega_g$ = 0.4
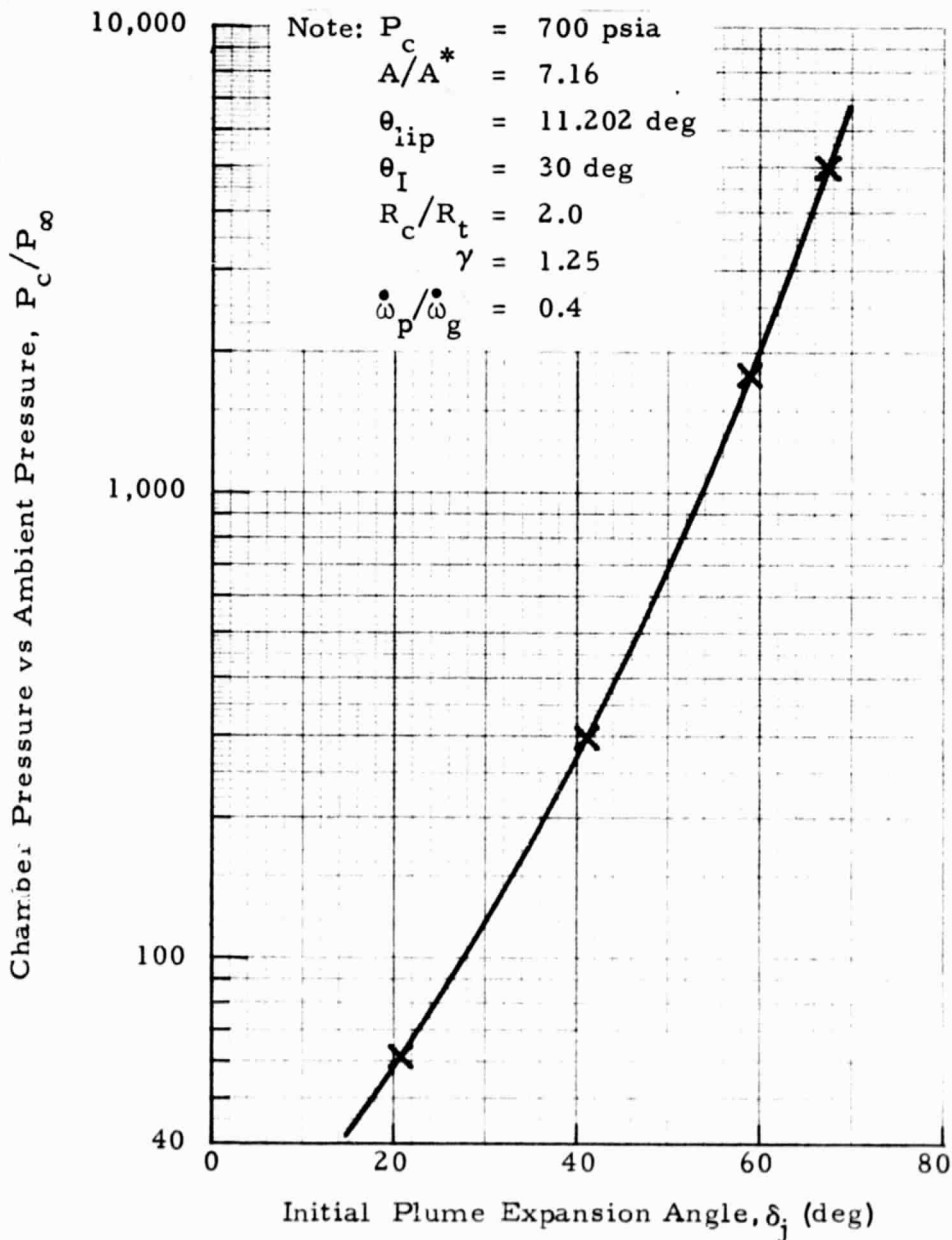
Fig. 9 - Variation of δ_j with Change in Ambient Pressure Ratio and Particle Distribution versus Mean Particle Size

28

r_{mp} \ P_c/P_∞	60	300	1800	5000
4	20.7	41.4	59.7	68.3
6	20.4	41.1	59.2	67.8
8	19.9	40.8	58.8	67.3

r_{mp}	P_c/P_e	M_e	$T_e(^oR)$
4	32.34	2.60	3275.2
6	33.11	2.62	3258.5
8	33.78	2.64	3244.0

Note: P_c = 700 psia
γ = 1.25
A/A^* = 7.16
$\dot{\omega}_p/\dot{\omega}_g$ = 0.4
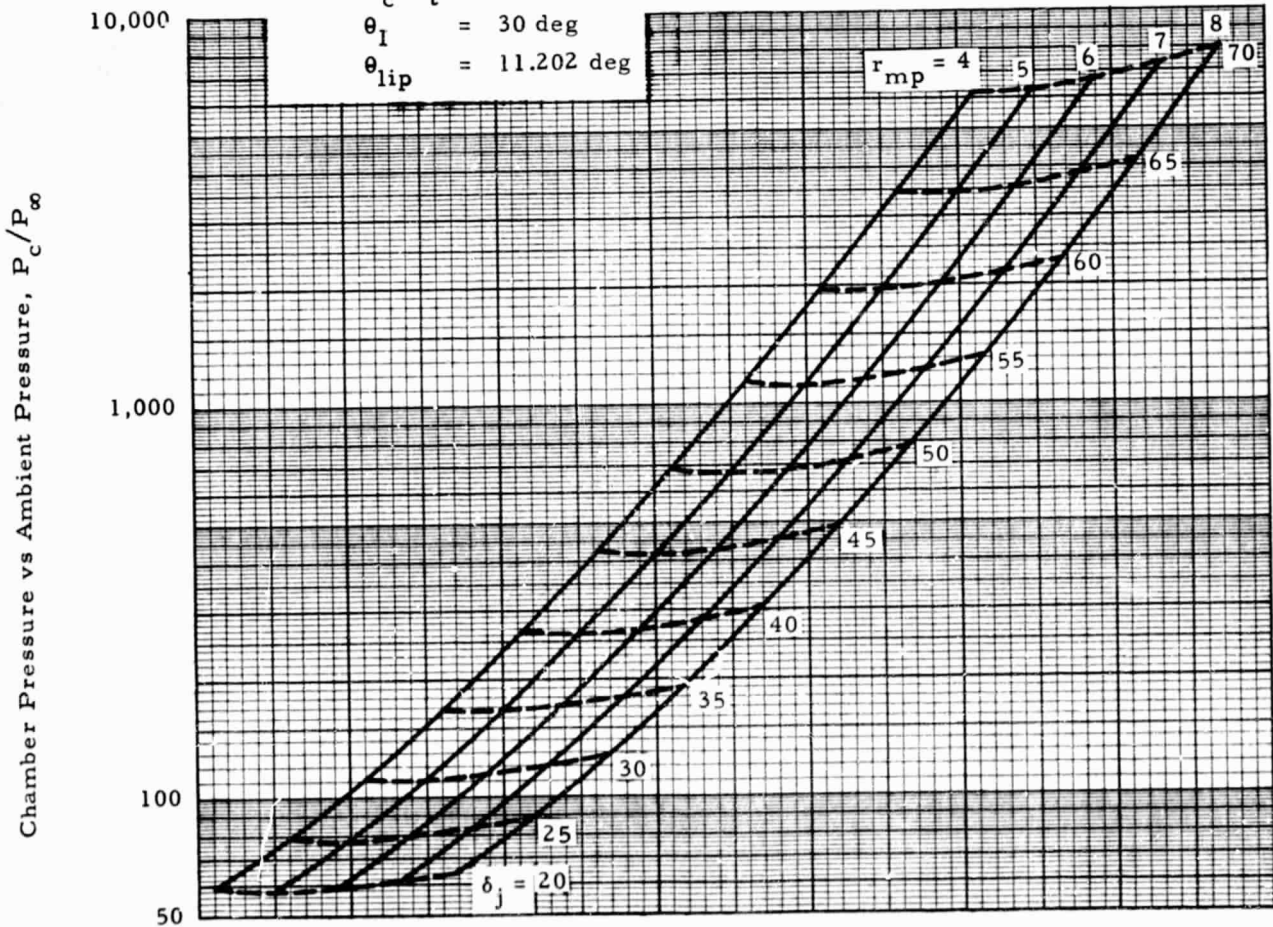R_c/R_t = 2.0
θ_I = 30 deg
θ_{lip} = 11.202 deg

Fig. 10 - Variation of δ_j with Change in P_c/P_∞ and Mass Mean Particle Size

29

r_{mp} \ P_c/P_∞	60	300	1800	5000
4	20.3	41.3	58.3	66.9
6	20.3	41.0	59.3	67.9
8	19.8	40.8	58.9	67.8

r_{mp}	P_c/P_e	M_e	$T_e(°R)$
4	32.610	2.60	3263.9
6	33.160	2.62	3248.2
8	33.715	2.63	3231.3

Note:
P_c = 700 psia
γ = 1.25
$\dot{\omega}_p/\dot{\omega}_g$ = 0.4
R_c/R_t = 2.0
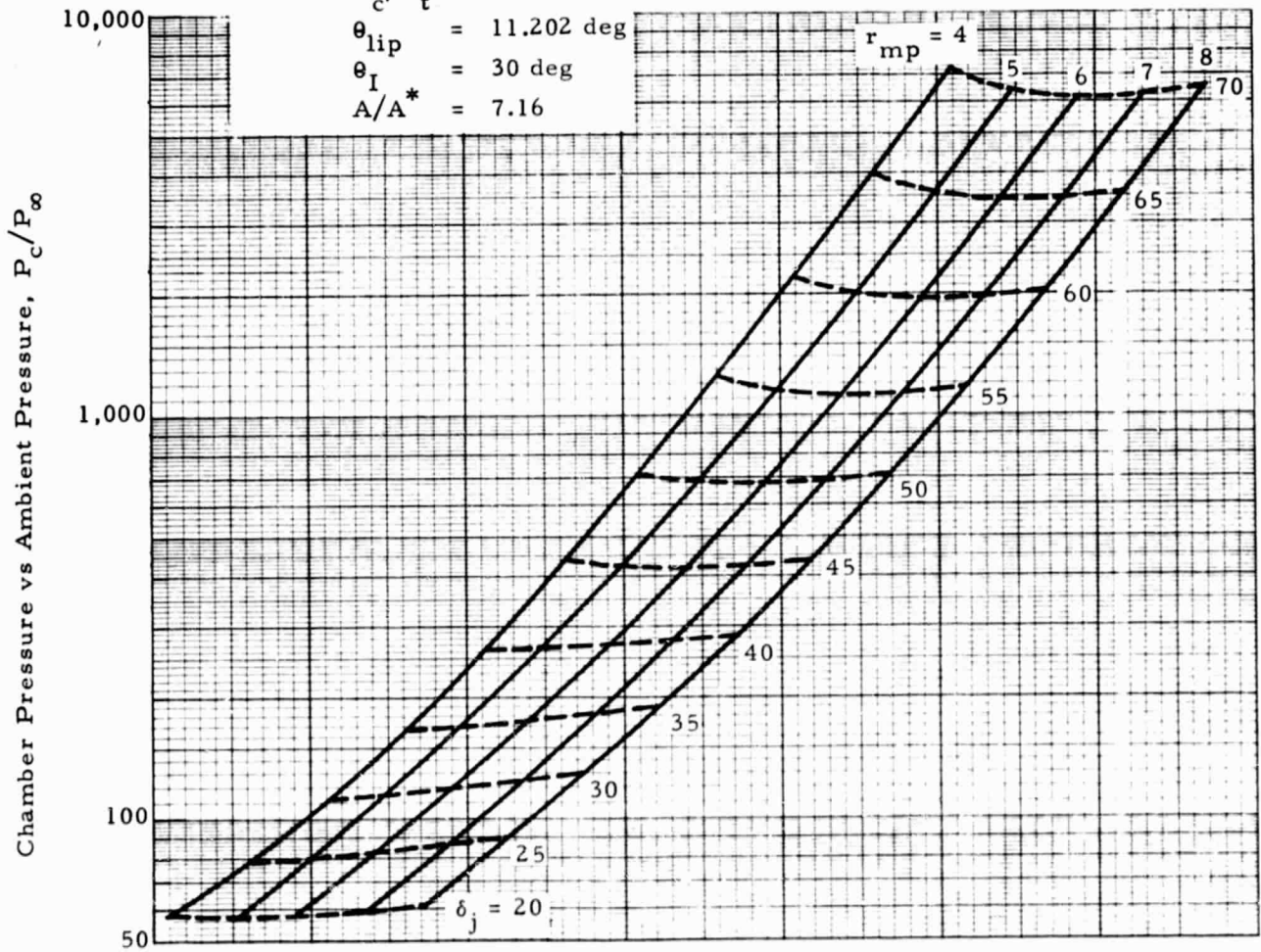θ_{lip} = 11.202 deg
θ_I = 30 deg
A/A^* = 7.16

Fig. 11 - Variation of δ_j with Change in Mass Mean Particle Size and Ambient Pressure Ratio for a Value of Twice the Local Kliegel Drag Coefficient

30

r_{mp} \ P_c/P_∞	60	300	1800	5000
4	20.2	41.0	59.4	67.9
6	20.2	41.0	59.4	67.9
8	19.5	40.0	58.3	66.9

r_{mp}	P_c/P_e	M_e	$T_e(°R)$
4	32.39	2.61	3282.1
6	33.27	2.63	3266.8
8	34.67	2.66	3241.8

Note: P_c = 700 psia
A/A^* = 7.16
θ_{lip} = 11.202 deg
θ_I = 30 deg
R_e/R_t = 2.0
γ = 1.25
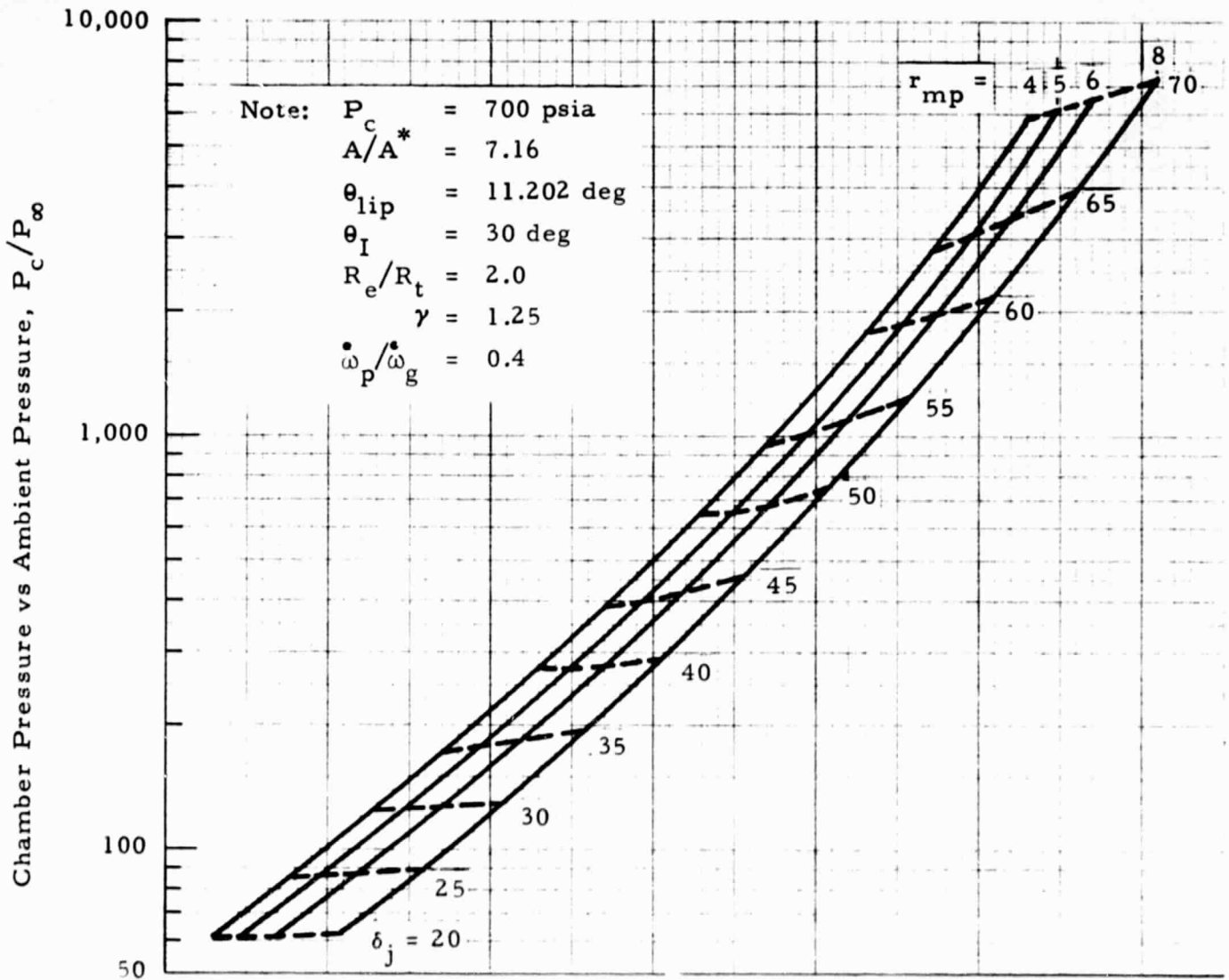$\dot{\omega}_p/\dot{\omega}_g$ = 0.4

Fig. 12 - Variation of δ_j with Change in Mass Mean Particle Size and Ambient
Pressure for a Value of One-Half the Local Kliegel Drag Coefficient

31

r_{mp} \ P_c/P_∞	60	300	1800	5000
4μ	19.7	40.8	59.9	68.3
6μ	20.6	41.3	59.7	68.4
8μ	20.1	41.0	59.3	67.9

r_{mp}	P_c/P_e	M_e	$T_e(^oR)$
4μ	33.55	2.64	3181.6
6μ	32.37	2.61	3282.6
8μ	32.68	2.62	3278.1

Note: P_c = 700 psia
A/A^* = 7.16
θ_{lip} = 11.202 deg
θ_I = 30 deg
R_c/R_t = 2.0
γ = 1.25
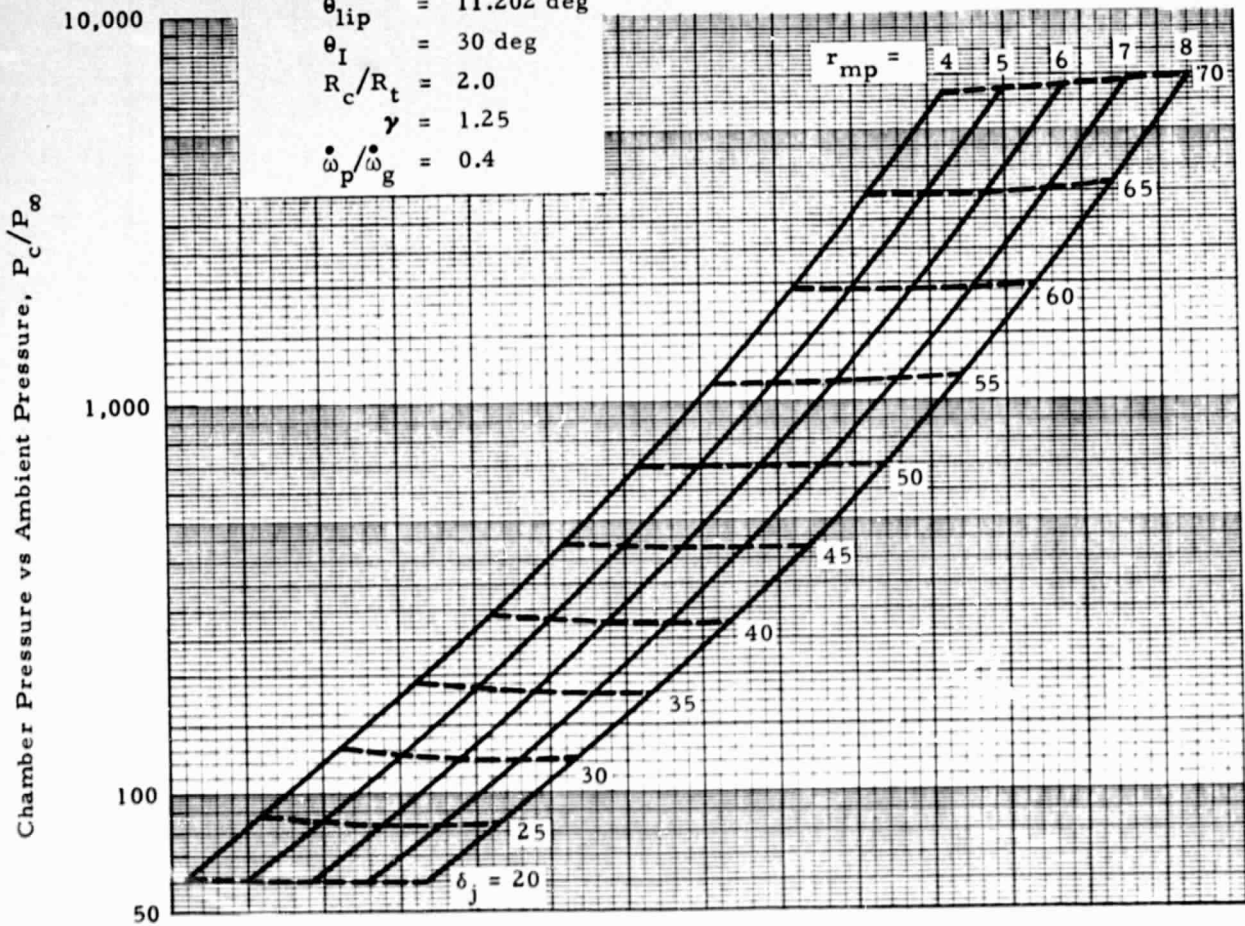$\dot{\omega}_p/\dot{\omega}_g$ = 0.4

Fig. 13 - Variation of δ_j with Change in Mass Mean Particle Size and Ambient Pressure for a Value of Twice the Local Heat Transfer Coefficient

32

r_{mp} \ P_c/P_∞	60	300	1800	5000
4μ	20.2	41.1	59.3	67.9
6μ	19.6	41.1	59.4	67.9
8μ	19.1	39.8	58.5	66.9

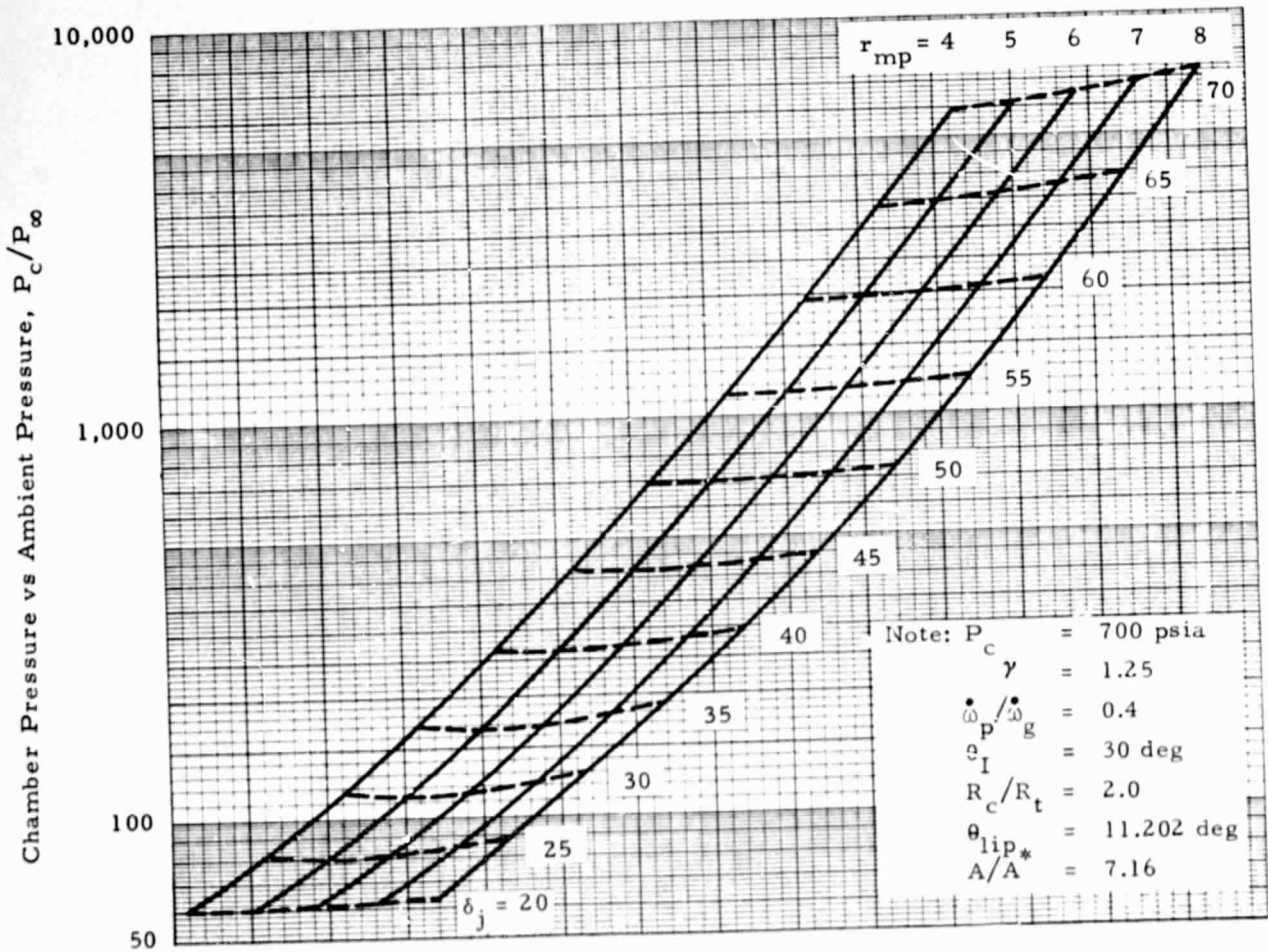| r_{mp}	P_c/P_e	M_e	$T_e (^{O}R)$
4μ	33.35	2.62	3244.6
6μ	34.47	2.64	3216.9
8μ	34.95	2.66	3202.6

Fig. 14 - Variation of δ_j with Change in Mass Mean Particle Size and Ambient Pressure Ratio for a Value of One-Half the Heat Transfer Coefficient of Drake

C_D \ P_c/P_∞	60	300	1800	5000
Kliegel	20.4	41.1	59.2	67.8
Crowe	20.1	40.9	59.2	67.8

C_D	P_c/P_e	M_e	$T_e(^oR)$
Kliegel	33.11	2.62	3258.5
Crowe	33.24	2.62	3257.2
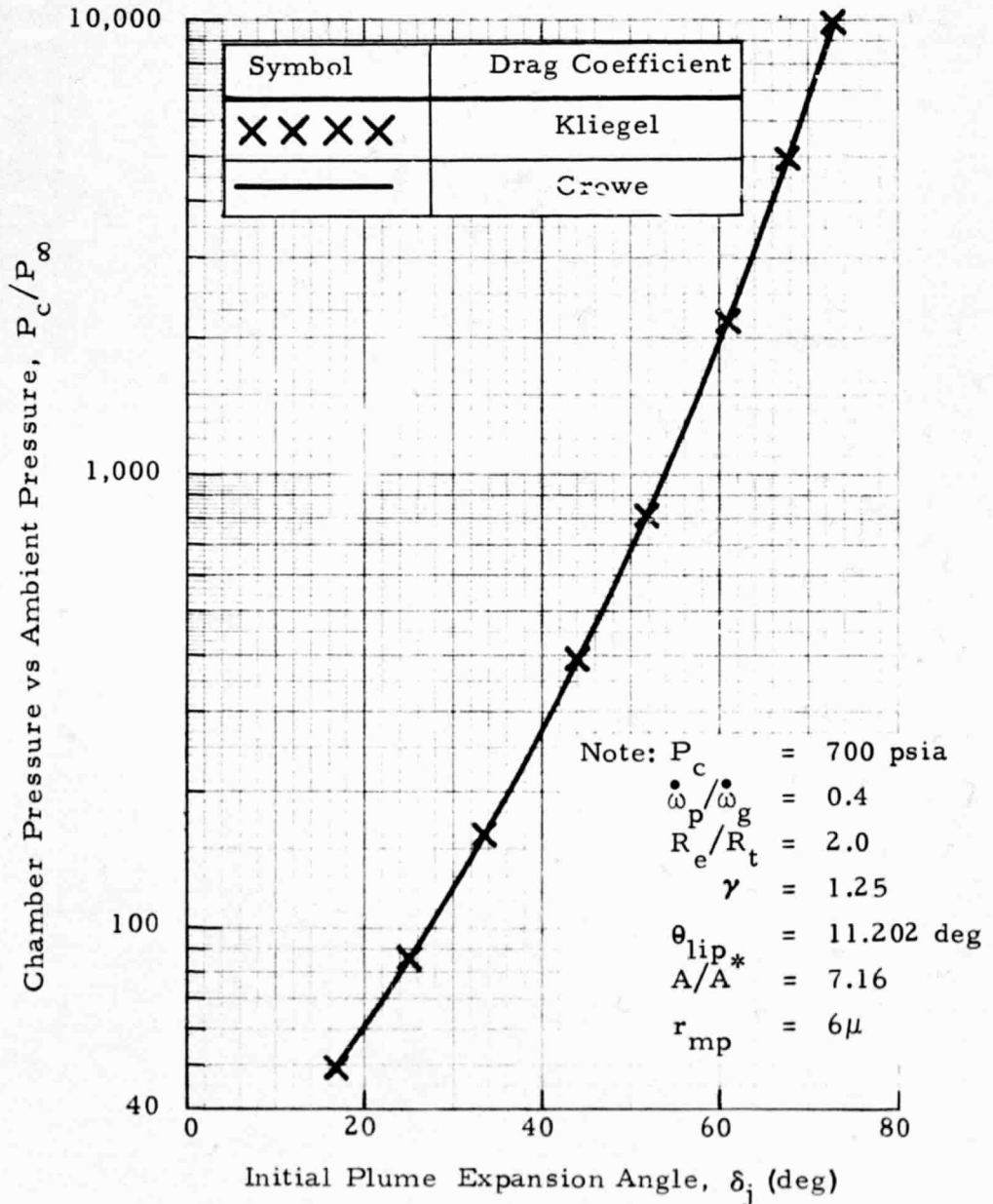
Fig. 15 - Variation of δ_j with Ambient Pressure Ratio for Two Drag Coefficient Calculations

34

C_D \ P_c/P_∞	60	300	1800	5000
$C_D \times 0.5$	20.2	41.0	59.4	67.9
$C_D \times 1.0$	20.4	41.1	59.2	67.8
$C_D \times 2.0$	20.3	41.0	59.3	67.9

C_D	P_c/P_e	M_e	$T_e(^\circ R)$
$C_D \times 0.5$	33.27	2.63	3266.8
$C_D \times 1.0$	33.11	2.62	3258.5
$C_D \times 2.0$	32.16	2.62	3248.0
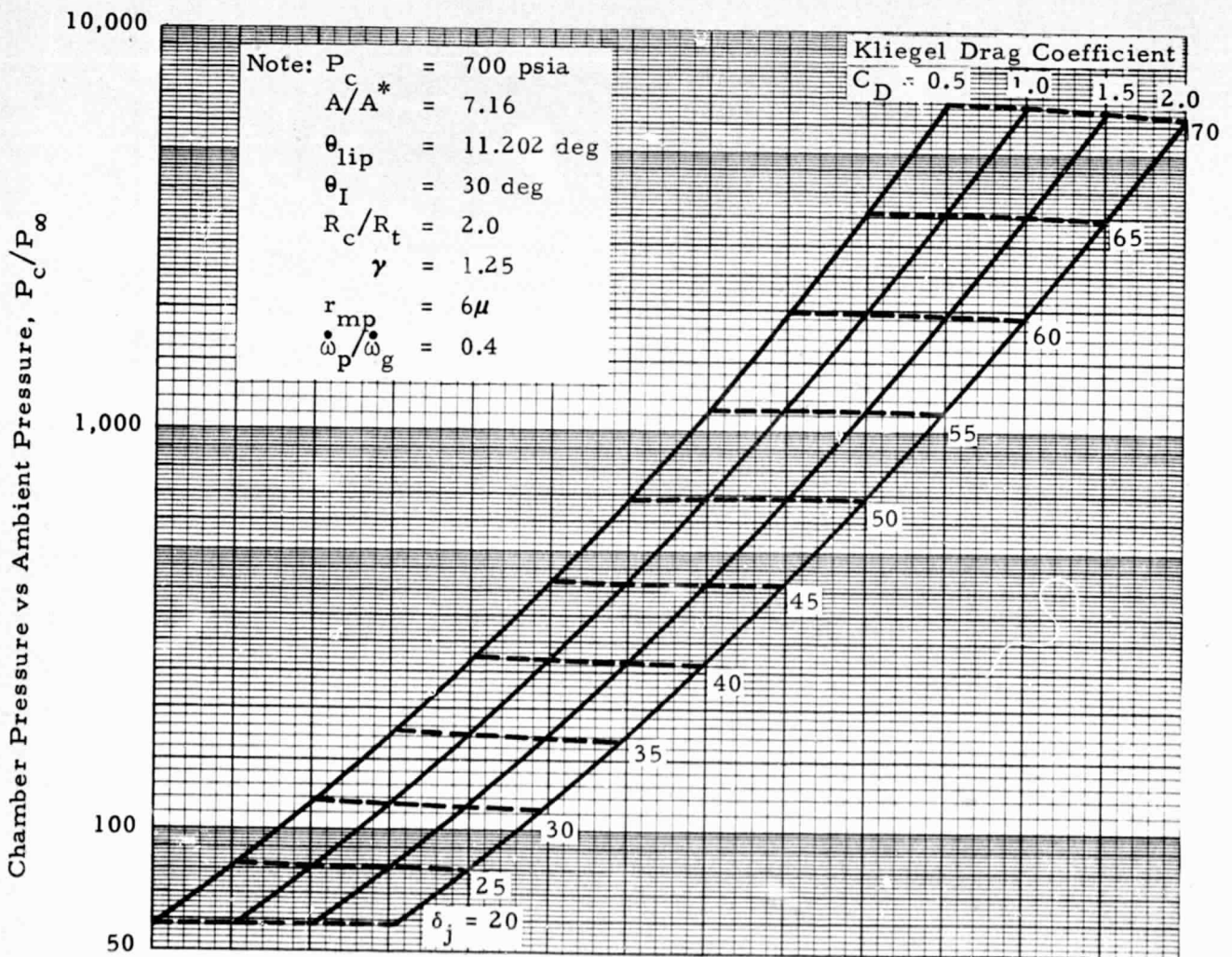
Fig. 16 - Variation of δ_j with Change in Local Drag Coefficient and Ambient Pressure Ratio

35

C_D	P_c/P_e	M_e	$T_e(^\circ R)$
Kliegel	33.48	2.63	3251.0
Crowe	33.60	2.63	3249.3

C_D $\diagdown$ P_c/P_∞	60	300	1800	5000
Kliegel	20.1	40.9	59.0	67.7
Crowe	19.8	40.8	58.9	67.6

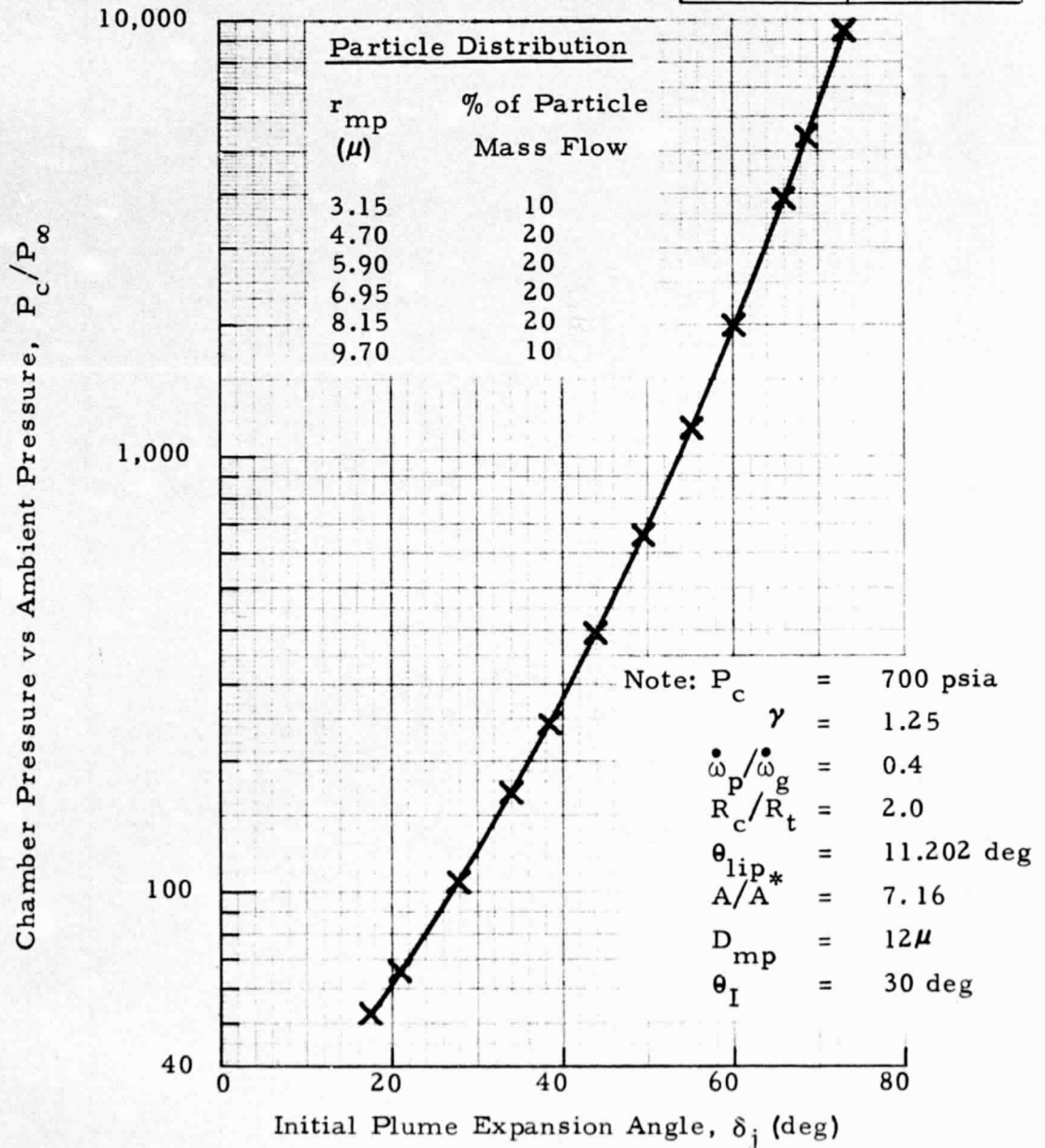| Symbol	Item
———	Kliegel
✕✕✕✕	Crowe

Fig. 17 - Variation of δ_j with Change in Drag Coefficient and Ambient Pressure Ratio including the Effects of Particle Size Distribution

36

C_D \\ P_c/P_∞	60	300	1800	5000
$C_D \times 0.5$	19.9	40.3	58.7	67.3
$C_D \times 1.0$	20.1	40.9	59.0	67.7
$C_D \times 2.0$	20.3	41.3	59.4	68.2

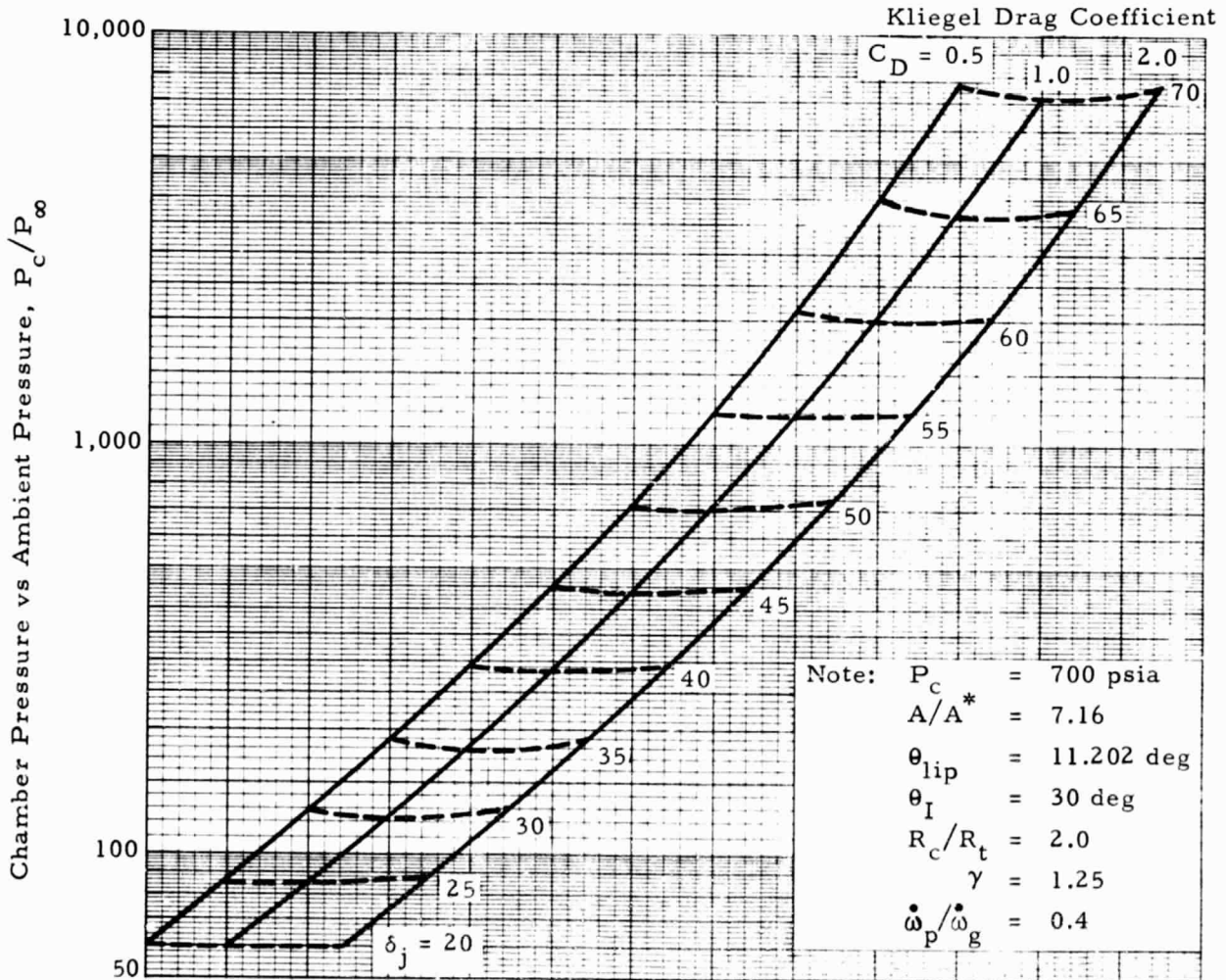| C_D	P_c/P_e	M_e	$T_e (^\circ R)$
$C_D \times 0.5$	33.82	2.64	3256.2
$C_D \times 1.0$	33.48	2.63	3251.0
$C_D \times 2.0$	32.61	2.60	3263.9

Fig. 18 - Variation of δ_j with Change in Drag Coefficient and Ambient Pressure Ratio Utilizing a Distribution of Particle Sizes

$\dot{Q}$ \ P_c/P_e	60	300	1800	5000
$\dot{Q}$x 0.5	19.6	40.1	58.5	67.1
$\dot{Q}$x 1.0	20.4	41.1	59.2	67.8
$\dot{Q}$x 2.0	20.6	41.3	59.7	68.4

$\dot{Q}$	P_c/P_e	M_e	$T_e(^oR)$
$\dot{Q}$x 0.5	34.46	2.64	3216.9
$\dot{Q}$x 1.0	33.11	2.62	3258.5
$\dot{Q}$x 2.0	32.37	2.61	3282.6

Fig. 19 - Variation of δ_j with Change in Local Heat Transfer
Coefficient and Ambient Pressure Ratio

38

$\dot{Q}x$	P_c/P_e	M_e	$T_e(^oR)$
0.5	33.55	2.64	3181.6
1.0	31.45	2.60	3236.4
2.0	28.89	2.57	3303.5

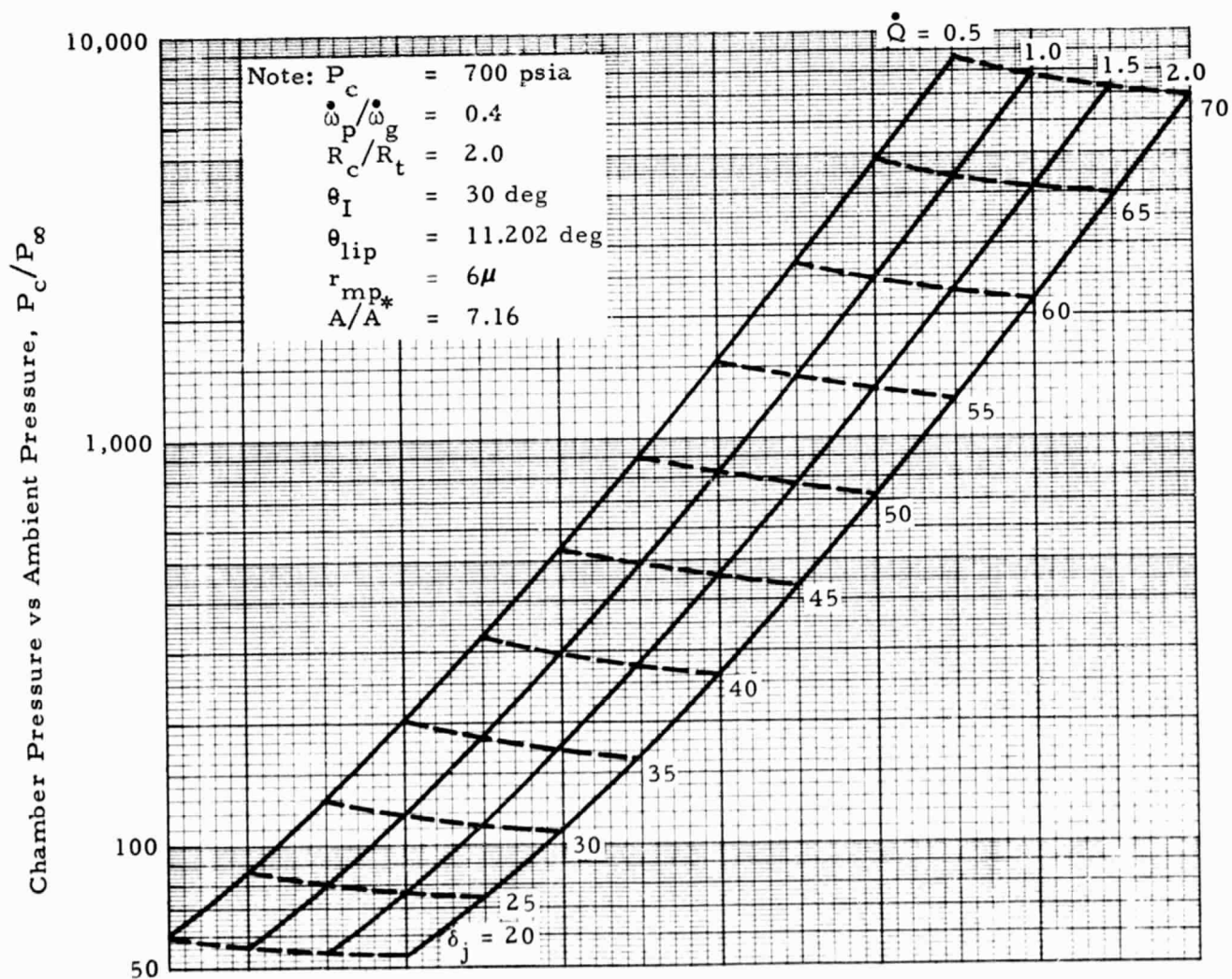| $\dot{Q}x$ ╲ P_c/P_∞	60	300	1800	5000
0.5	19.9	39.2	56.4	65.5
1.0	20.9	40.2	57.1	66.2
2.0	22.1	41.4	58.2	67.3

Fig. 20 - Variation of δ_j with Change in Heat Transfer Coefficient and Ambient Pressure Ratio Assuming Chemically Frozen Flow from the Nozzle Throat

39

$\dot{Q}x$	P_c/P_e	M_e	$T_e(^oR)$
0.5	32.83	2.62	3273.7
1.0	33.11	2.62	3258.5
2.0	34.40	2.64	3217.5

$\dot{Q}x$ \ P_c/P_∞	60	300	1800	5000
0.5	19.9	40.25	58.6	67.1
1.0	20.1	40.90	59.0	67.7
2.0	20.5	41.10	59.3	67.9

Note:
P_c = 700 psia
A/A^* = 7.16
θ_{lip} = 11.202 deg
θ_I = 30 deg
R_c/R_t = 2.0
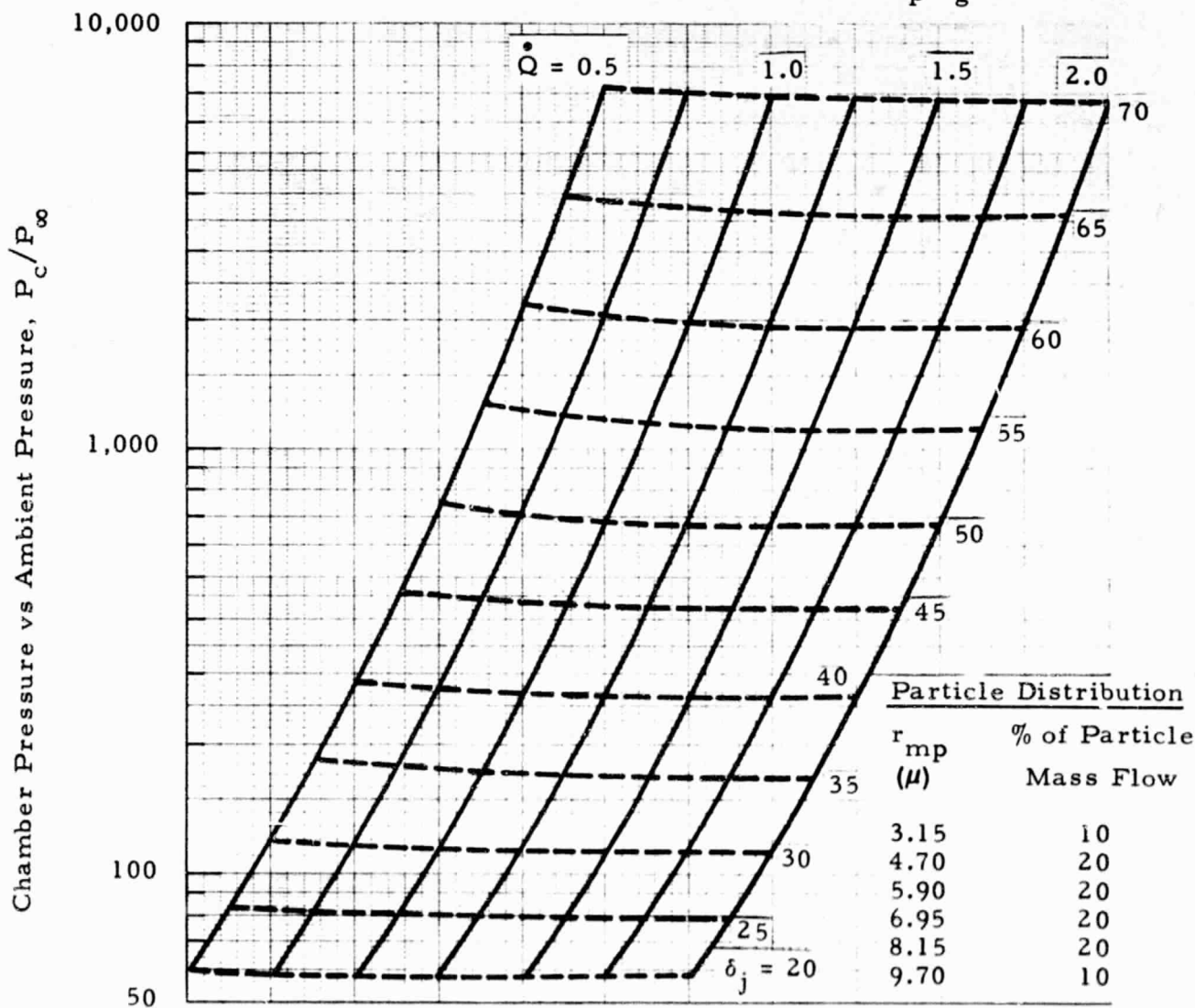γ = 1.25
$\dot{\omega}_p/\dot{\omega}_g$ = 0.4

Fig. 21 - Variation of δ_j with Change in Local Heat Transfer Coefficient and Ambient Pressure Ratio Including The Effects of Particle Size Distribution

40

Item	P_c/P_e	M_e	$T_e(°R)$
————	34.46	2.64	3216.9
– – – –	33.11	2.62	3248.2
—·—·—	32.22	2.60	3277.4

Symbol	Item
————	$0.5\,\dot{Q},\ C_D$
– – – –	Nominal
—·—·—	$2\,C_D,\ 2\dot{Q}$

Note: P_c = 700 psia
A/A^* = 7.16
θ_{lip} = 11.202 deg
θ_I = 30 deg
R_c/R_t = 2.0
γ = 1.25
r_{mp} = 6μ
$\dot{\omega}_p/\dot{\omega}_g$ = 0.4

Chamber Pressure vs Ambient Pressure, P_c/P_∞

Initial Plume Expansion Angle, δ_j (deg)
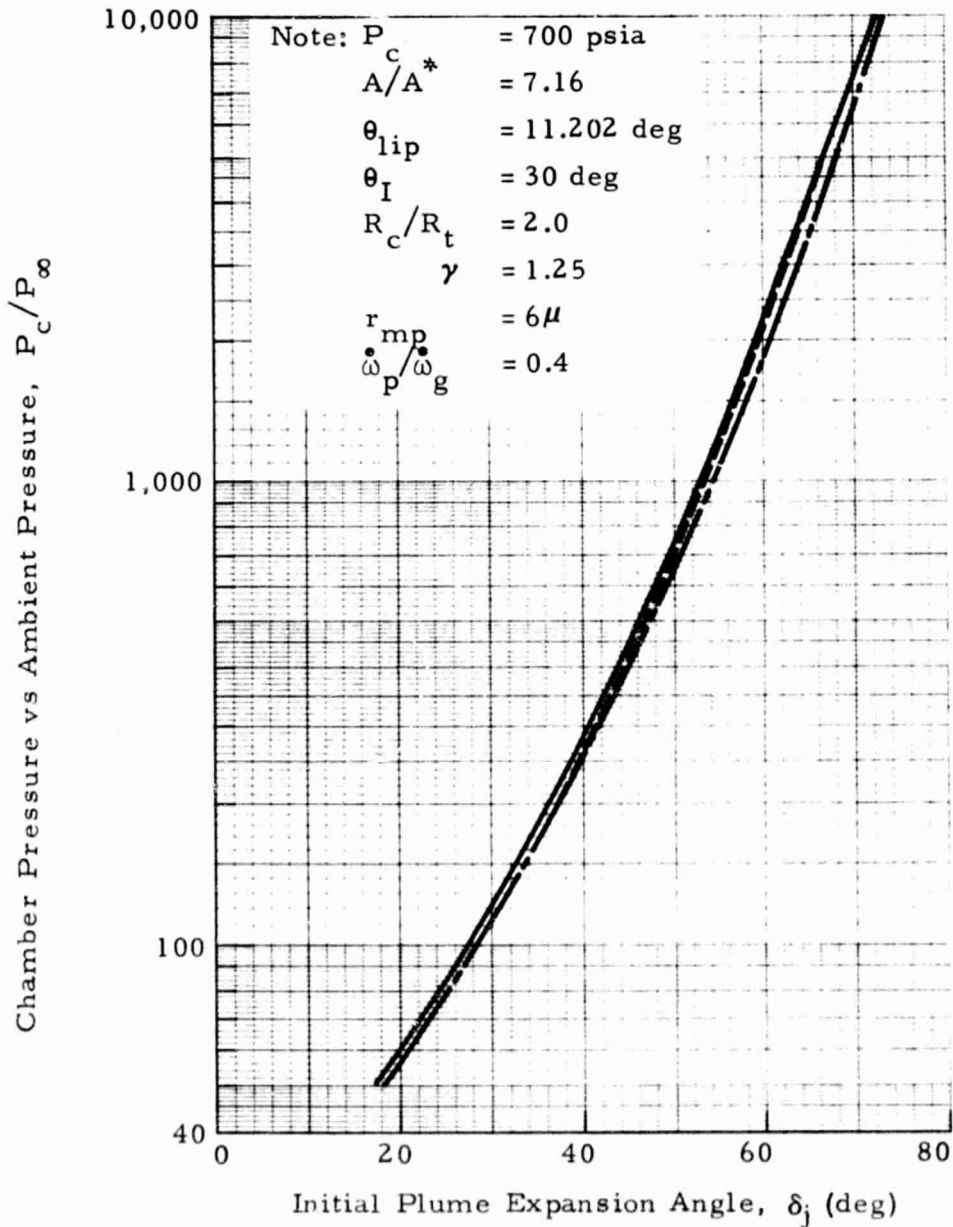
Fig. 22 - Variation of δ_j with Change in Particle Drag
and Heat Transfer Coefficients

41

Item	P_c/P_e	M_e	$T_e(^oR)$
✗ ✗ ✗ ✗	33.11	2.62	3248.2
– – – –	32.22	2.60	3277.4
———	33.27	2.63	3216.9

Symbol	Item
✗ ✗ ✗ ✗	Nominal
– – – –	$2C_D$, $2\dot{Q}$
———	$0.5C_D$, $\dot{Q}$

Note: P_c = 700 psia
A/A^* = 7.16
θ_{lip} = 11.202 deg
θ_I = 30 deg
R_c/R_t = 2.0
γ = 1.25
r_{mp} = 6μ
$\dot{\omega}_p/\dot{\omega}_\xi$ = 0.4
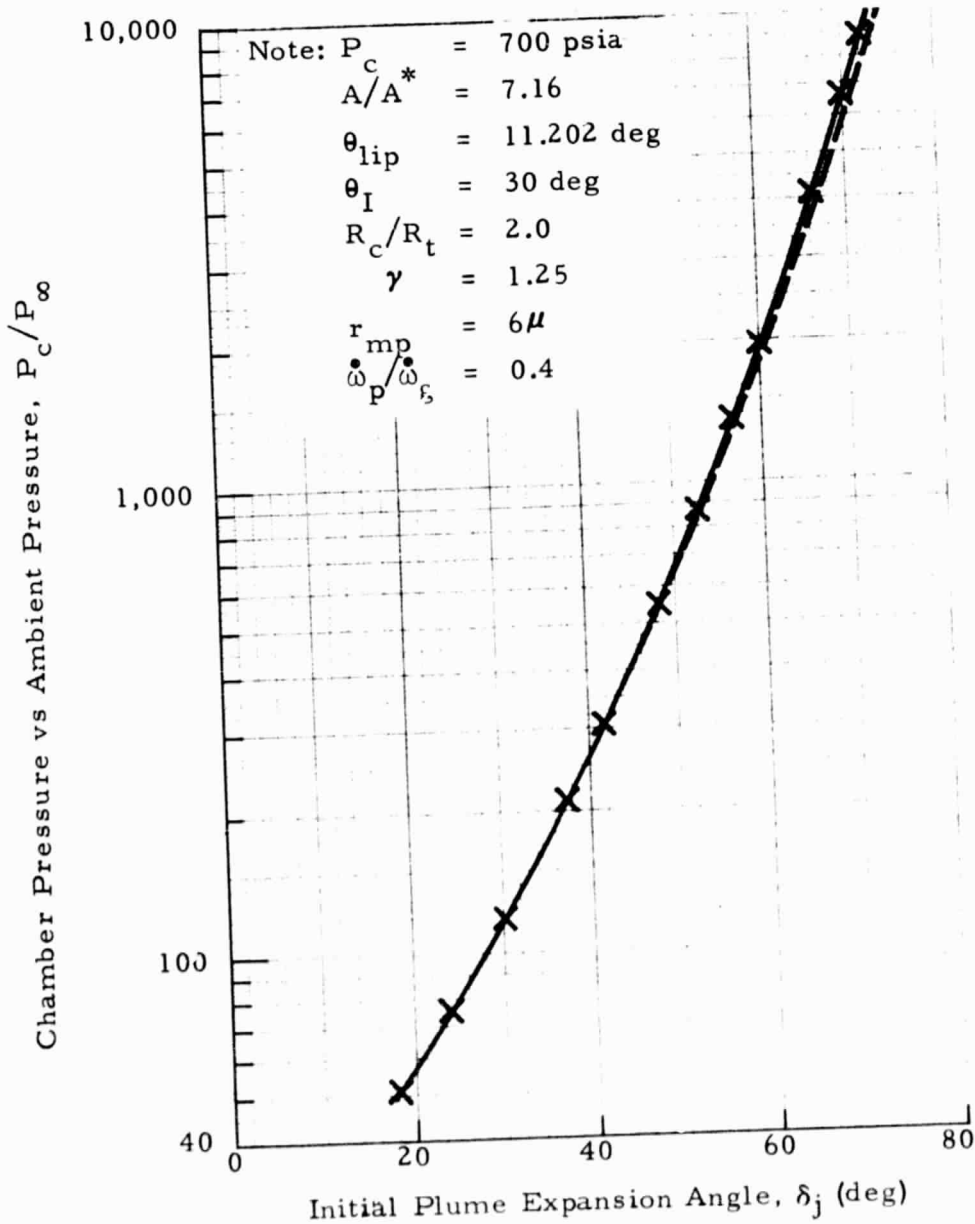
Fig. 23 - Variation of δ_j with Change in Particle Drag
and Heat Transfer Coefficients

42

Symbol	Item
——————	$2C_D, \dot{Q}$
X X X	$2C_D, 2\dot{Q}$
— — —	Nominal

Item	P_c/P_e	M_e	$T_e(°R)$
$2C_D, \dot{Q}$	33.17	2.62	3248.2
$2C_D, 2\dot{Q}$	32.22	2.60	3277.4
Nominal	33.11	2.62	3258.5

Note: P_c = 700 psia

$A/A^* = 7.16$

θ_{lip} = 11.202 deg

θ_I = 30 deg

R_e/R_t = 2.0

γ = 1.25

r_{mp} = 6μ

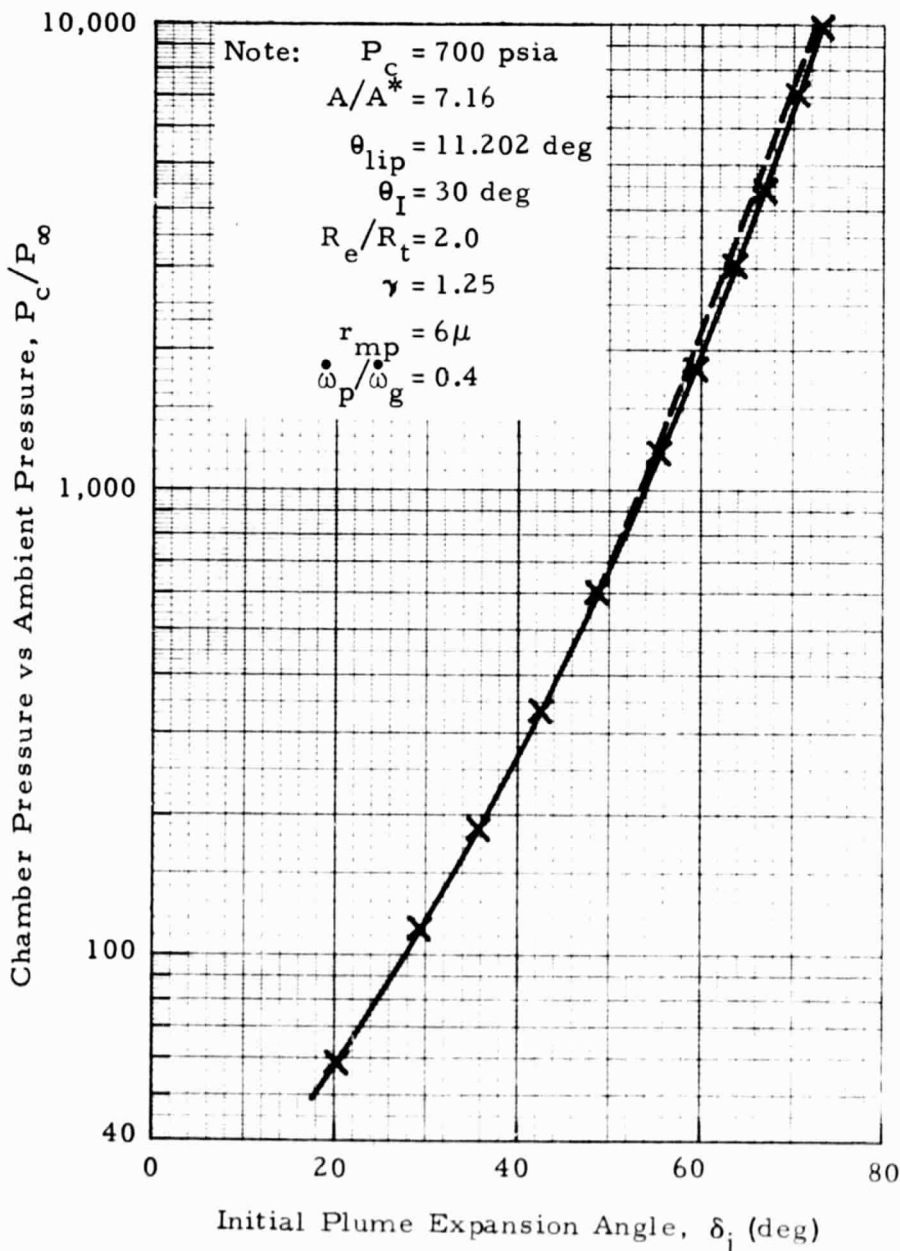$\dot{\omega}_p/\dot{\omega}_g$ = 0.4

Fig. 24 - Variation of δ_j with Change in Particle Drag and Heat Transfer Coefficients

43